

# Vertical structure and stability of accretion discs with convective energy transport and external X-ray irradiation.

A. S. Tavleev,<sup>\*</sup> G. V. Lipunova, and K. L. Malanchev

*Sternberg Astronomical Institute, Moscow M. V. Lomonosov State University, 13 Universitetski pr., 119234, Moscow, Russia*

Accepted XXX. Received YYY; in original form ZZZ

## ABSTRACT

Radial structure of accretion discs around compact objects is usually described using analytic approximations which are derived from averaging or integrating vertical structure equations. For non-solar chemical composition, partial ionization, or for supermassive black holes, this approach is not accurate. Additionally, radial extension of ‘analytically-described’ disc zones is not evident in many cases. We calculate vertical structure of accretion discs around compact objects, with and without external irradiation, with radiative and convective energy transport taken into account. For this, we introduce a new open Python code, allowing different equations of state (EoS) and opacity laws, including tabular values. As a result, radial structure and stability ‘S-curves’ are calculated for specific disc parameters and chemical composition.

Consequently, we check the standard division of discs into zones A, B and C, depending on the role of radiation pressure and the main opacity mechanism. For the farthest regions of the hot disc around stellar-mass object we supply new analytic formulas. For discs around supermassive black holes, specific zone B\* appears, a mixture of A and C zones.

On calculating vertical structure of a self-irradiated disc, we are able to obtain a self-consistent value of the irradiation parameter  $C_{\text{irr}}$ . We find that  $C_{\text{irr}}$  depends weakly on the accretion rate but changes with radius, and the dependence is driven by the conditions in the photosphere and disc opening angle. The hot zone extent depends on the ratio between irradiating and intrinsic flux: corresponding relation for  $T_{\text{irr, crit}}$  is obtained.

**Key words:** accretion, accretion discs – instabilities – X-rays: binaries

## 1 INTRODUCTION

Disc accretion is a common astrophysical phenomenon widely observed thanks to high efficiency of energy emission. Brightest sources of the X-ray sky are explained by accretion of matter on compact objects, and visibility of such sources allows us to investigate physics operating there. Many X-ray sources are found in binary systems since the matter can flow from one component to another. Having large specific angular momentum, the matter forms an accretion disc.

The standard model of viscous accretion discs (Shakura 1972; Shakura & Sunyaev 1973) is based on the notion of the turbulent viscosity as a mechanism for the angular momentum transfer, allowing the matter, rotating around a central object, to move inwards and to emit gravitational energy converted to heat. Heat balance determines the vertical structure of the disc, that is, in the direction perpendicular to its symmetry plane. It is safe to assume that hydrostatic equilibrium holds in the vertical direction, meaning that the time to achieve the hydrostatic balance is much shorter than other characteristic disc times. The thermal balance in the vertical direction occurs on a time-scale longer than a hydrostatic one, but faster than the disc evolves due to accretion rate variations. Thus, generally, the vertical disc structure could be studied separately from the radial one.

Considering accretion onto compact object of stellar masses, it is commonly assumed that the standard model describes well the disc

regions that emit mainly in the optical. In this context, the details of the disc vertical structure are important since they determine the brightness and spectra of those regions.

It has been known for some time that the vertical structure of accretion disc is subject to various instabilities. The most studied are the instability with respect to fluctuations in the surface density of the disc (viscous one) and instability with respect to temperature fluctuations (thermal one), see e.g. Kato et al. (2008) for a review.

Thermal instability could be a cause of outbursts occurring rather periodically in some sources with accretion discs. A model based on disc instabilities has been developed in a number of works (e.g., Hōshi (1979); Smak (1982a); Meyer & Meyer-Hofmeister (1981, 1982); Faulkner et al. (1983); Papaloizou et al. (1983); Smak (1984)). Presently, it is referred to as the Disc Instability Model (or DIM, Hameury et al. 1998; Lasota 2001; Hameury 2020), see also Bagińska et al. (2021). Details of DIM depend not only on the disc vertical structure at different radii but on the radial energy transport as well. To some extent, using the local analysis alone, it is possible to study the scenario with thermal-viscous instability on a basis of so-called S-curves (Meyer & Meyer-Hofmeister 1981), or equilibrium curves. An S-curve is a graphically depicted sequence of solutions of the vertical-structure equations, obtained at a single disc radius, in the coordinates of accretion rate or effective temperature versus the surface density (see Fig. 10 below). The positive slope of an S-curve represents the thermally and viscously stable state of the disc, whereas the negative slope represents the unstable state.

\* E-mail: tavleev.as15@physics.msu.ru

In X-ray transients, burst evolution depends crucially on the self-irradiation of the disc: heating by central X-rays can change the local state of the outer disc and, thus, the viscosity there (Tuchman et al. 1990; Dubus et al. 2001). Vertical structure of a self-irradiated  $\alpha$ -disc has been calculated by Tuchman et al. (1990); Dubus et al. (1999), who introduced a self-irradiation parameter. Self-consistent calculations of the vertical structure of irradiated discs have been performed by Mescheryakov et al. (2011) for fully ionized disc regions with opacity from the Opacity Project (Badnell et al. 2005).

In the current paper, we present results for disc vertical structure obtained with our new open Python code with modern values of opacity (Iglesias & Rogers 1993, 1996; Ferguson et al. 2005) and equations of state (Rogers & Nayfonov 2002)<sup>1</sup>. We take into account X-ray irradiation by two methods and vertical transfer of energy by convection using an approach of the mixing-length theory. The code uses MESA package (Paxton et al. 2011) for interpolation and sewing of the opacity and EoS tables. It can calculate the vertical structure, S-curves, and radial profiles of optically thick accretion discs.

For un-irradiated discs, we analyse physical conditions in the discs for a wide range of parameters. We examine to what extent analytical approximations for opacity laws, and, consequently, for radial dependencies, can be satisfactorily used. We study ionization degree in the vertical direction and its behavior in unstable states.

We analyse stability conditions for un-irradiated and self-irradiated discs. For self-irradiated discs, we also calculate the value of the self-irradiation parameter in the thermally stable disc parts, and analyse its dependence on the basic parameters of accretion disc.

In section 2, we present a system of equations of the vertical structure and boundary conditions, in particular, in the presence of external X-ray irradiation, and give examples of its integration by the new code in section 3. The radial structure of the disc, resulting from solutions for vertical structure, is investigated in section 4. The irradiation parameter is considered there as well. In section 5, we construct and analyse S-curves. In section 6 we analyse and discuss the stability criterion of the irradiated disc. Summary is given in section 7.

Appendices A and B review equations used in presence of convective energy transport and external X-ray disc irradiation. Examples of the vertical structure of irradiated disc are described in Appendix C. Appendices D and E contain a brief description of the code and details of the calculation scheme we use.

## 2 MODELLING OF ACCRETION DISC VERTICAL STRUCTURE

We use a cylindrical coordinate system  $(r, \varphi, z)$ , where  $z$  changes from 0 in the symmetry plane to the semi-thickness of disc  $z_0$  on the disc surface. We consider geometrically thin ( $z_0 \ll r$ ) Keplerian ( $\omega = \omega_K = \sqrt{GM/r^3}$ ) stationary ( $\partial/\partial t = 0$ ) optically thick ( $\tau \gg 1$ ) accretion disc.

In such discs, the characteristic viscous time (the time it takes for accretion rate to change) is much greater than the characteristic dynamic time (the time it takes for pressure to change) and the characteristic thermal time (the time it takes for the thermal energy

to change):

$$\begin{aligned} t_{\text{vis}} &\sim \frac{r}{|v_r|} \sim \frac{1}{\alpha\omega} \left(\frac{z_0}{r}\right)^{-2}, & t_{\text{dyn}} &\sim \frac{z_0}{v_s} \sim \frac{1}{\omega}, \\ t_{\text{th}} &\sim \frac{\epsilon}{\dot{\epsilon}} \sim \frac{1}{\alpha\omega}, & t_{\text{vis}} &\gg t_{\text{dyn}}, & t_{\text{vis}} &\gg t_{\text{th}}, \end{aligned} \quad (1)$$

where  $v_r$  and  $v_s$  are radial and sound velocity,  $\epsilon$  is the amount of energy dissipating per unit volume per unit time and  $\alpha$  is the turbulent parameter (see below). With such characteristic times, the vertical structure equations can be decoupled from the radial structure ones.

The vertical structure of  $\alpha$ -discs has been solved in a number of papers, including Smak (1984); Meyer & Meyer-Hofmeister (1982); Hameury et al. (1998); Lasota et al. (2008) where discs in X-ray transients were considered in particular. Note that they used previous values of opacity (Cox & Stewart 1969; Cox & Tabor 1976; Alexander 1975) and EoS (Fontaine et al. 1977). Ketsaris & Shakura (1998); Suleimanov et al. (2007); Malanchev et al. (2017) have solved the vertical structure with analytical opacity coefficient and equation of state, which allows obtaining analytical radial structure (see Sect. 4).

### 2.1 Basic equations

Vertical structure equations follow from the mass, energy and momentum conservation laws. In the discs with moderate accretion rates and small temperature gradients along the radius, the energy balance is local: there is virtually no energy transfer in the radial direction. First we consider discs without external heating by irradiation.

(i) The disc is assumed to be in hydrostatic equilibrium along the vertical coordinate  $z$ :

$$\frac{dP}{dz} = -\rho \omega_K^2 z. \quad (2)$$

where  $P$  and  $\rho$  are the gas pressure and density.

Note that in general the influence of radiation pressure  $P_{\text{rad}}$  should be taken into account (in that case  $P = P_{\text{gas}} + P_{\text{rad}}$ ). The well-known type of instability appears when  $P_{\text{rad}} \gg P_{\text{gas}}$  (Lightman & Eardley 1974; Shakura & Sunyaev 1976). This instability manifests itself as a poor convergence of the structure solution of our numerical scheme. Thus, we consider those parts of disc, where the radiation pressure  $P_{\text{rad}} \ll P_{\text{gas}}$  and can be neglected.

(ii) The disc is heated by viscosity caused by turbulent motions, i.e. the energy heating flux  $Q = Q_{\text{vis}}$ , where  $Q_{\text{vis}}$  is the energy flux due to viscosity. Equation of viscous heating rate:

$$\frac{dQ}{dz} = \frac{dQ_{\text{vis}}}{dz} = -w_{r\varphi} r \frac{d\omega}{dr} = \frac{3}{2} w_{r\varphi} \omega_K, \quad (3)$$

where  $w_{r\varphi}$  is the absolute value of the  $r\varphi$ -component of tensor of viscous tensions. We use the  $\alpha$ -prescription (Shakura & Sunyaev 1973), where  $w_{r\varphi} = \alpha P$ , and  $\alpha$  is the turbulent parameter ( $0 < \alpha < 1$ ):

$$\frac{dQ}{dz} = \frac{3}{2} \omega_K \alpha P. \quad (4)$$

External X-ray irradiation can be another source of disc heating. In this case the heating flux  $Q = Q_{\text{vis}} + Q_{\text{irr}}$  (see Sect. 2.4 below).

(iii) Generally, the heat is transported in vertical direction by radiation and convection. We define temperature gradient as follows (Meyer & Meyer-Hofmeister 1982):

$$\frac{d \ln T}{d \ln P} \equiv \nabla = \begin{cases} \nabla_{\text{rad}}, & \nabla_{\text{rad}} \leq \nabla_{\text{ad}}, \\ \nabla_{\text{conv}}, & \nabla_{\text{rad}} \geq \nabla_{\text{ad}}, \end{cases} \quad (5)$$

<sup>1</sup> Opacities of Iglesias & Rogers (1993, 1996) and Badnell et al. (2005) differs by up to 10% in area of typical disc parameters.

where  $\nabla_{\text{rad}}$  is the radiative gradient,  $\nabla_{\text{ad}}$  is adiabatic gradient and  $\nabla_{\text{conv}}$  is the gradient when both convection and radiation occur. If the radiative gradient is overadiabatic, the convection takes place (Schwarzschild criteria, [Schwarzschild 1958](#)).

If  $\nabla_{\text{rad}} \leq \nabla_{\text{ad}}$ , the energy is transported by radiation, and the temperature gradient follows from the radiation transfer equation in diffusion approximation and is as follows

$$\nabla_{\text{rad}} \equiv \frac{3\kappa_{\text{R}}}{4ac\omega_{\text{K}}^2 z} \frac{P}{T^4} Q, \quad (6)$$

where  $\kappa_{\text{R}}$  is the Rosseland opacity coefficient,  $a = 4\sigma_{\text{SB}}/c$  is the radiation constant,  $c$  is the speed of light, and the cooling flux is equal to heating flux  $Q$ , because there is no advection in the disc (no radial energy transport).

If  $\nabla_{\text{rad}} \geq \nabla_{\text{ad}}$ , the convective motions start to transfer energy, and the corresponding temperature gradient  $\nabla_{\text{conv}}$  is calculated according to the mixing length theory (see [Paczynski 1969](#); [Kippenhahn et al. 2012](#)), see Appendix A. This approach to include convective transport of energy was also used by ([Hameury et al. 1998](#)), while ([Malanchev & Shakura 2015](#)) took an attempt to take into account exceed viscous energy generation in convective cells. Notice that in presence of convection  $\nabla_{\text{rad}} > \nabla_{\text{conv}} > \nabla_{\text{ad}}$ .

Finally, the temperature equation we shall solve is

$$\frac{dT}{dz} = \nabla \frac{T}{P} \frac{dP}{dz}. \quad (7)$$

In some calculation runs, for the sake of comparison, we formally calculate the disc structure always setting  $\nabla = \nabla_{\text{rad}}$ . We call such models ‘no convection’.

(iv) Surface density of disc is defined as

$$\Sigma_0 \equiv \int_{-z_0}^{+z_0} \rho(z) dz = 2 \int_0^{z_0} \rho(z) dz. \quad (8)$$

We also introduce mass coordinate  $\Sigma(z)$ , the column density ‘‘accumulated’’ from equatorial plane to a certain height  $z$  in both directions. We count this coordinate from the surface to the symmetry plane, which leads to the appearance of a ‘‘minus’’ sign in the equation for  $\Sigma$ :

$$\frac{d\Sigma}{dz} = -2\rho. \quad (9)$$

Subsequently, the surface density of the disc is  $\Sigma_0 = \Sigma(z=0)$ .

## 2.2 Equation of state and opacity law

System of four ordinary differential equations (2), (4), (7) and (9) should be supplemented by equation of state (EoS) and opacity law:

$$\rho = \rho(P, T), \quad \kappa_{\text{R}} = \kappa_{\text{R}}(\rho, T). \quad (10)$$

They can be set both analytically or as tabular values. For analytical description, the ideal gas equation is adopted:

$$\rho = \frac{\mu P}{\mathcal{R}T} \quad (11)$$

where  $\mu$  is molecular weight.

An analytic opacity coefficient is approximated by a power-law function:

$$\kappa_{\text{R}} = \kappa_0 \rho^\zeta T^\gamma. \quad (12)$$

Here  $\kappa_0$  is the dimension constant, which we give below in CGS units.

There are following analytic opacity options:

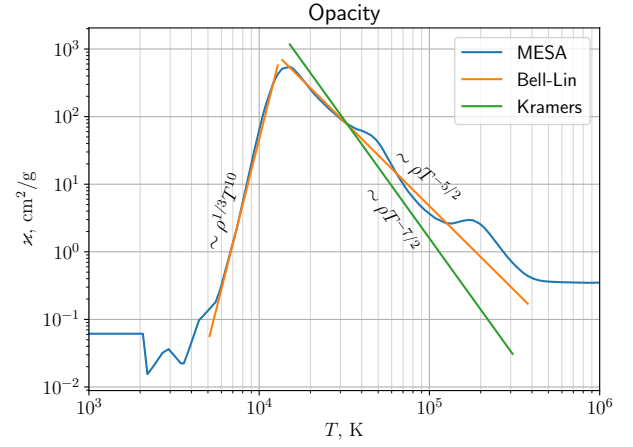


**Figure 1.** Rosseland opacity coefficient as a function of temperature for different opacity models for solar chemical composition and  $\rho = 10^{-7} \text{ g cm}^{-3}$ . Blue line shows interpolation of the tabular values (see Sect. 2.2). Orange and green lines correspond to Kramers ([Frank et al. 2002](#)) and Bell & Lin (1994) power-law approximations, respectively.

- Kramers law, which describes bound-bound and free-free transitions in the plasma ([Frank et al. 2002](#)):  $\zeta = 1$ ,  $\gamma = -7/2$ . For solar chemical composition  $\kappa_0 = 5 \cdot 10^{24}$ .

- Analytic approximations by Bell & Lin (1994) to opacity: approximation obtained by the OPAL project ([Iglesias & Rogers 1993](#)) ( $\kappa_0 = 1.5 \cdot 10^{20}$ ,  $\zeta = 1$ ,  $\gamma = -5/2$ ) and opacity from scattering off hydrogen atoms ( $\kappa_0 = 1 \cdot 10^{-36}$ ,  $\zeta = 1/3$ ,  $\gamma = 10$ ).

At high temperature the analytical opacity is determined by the Thomson electron scattering, i.e.  $\kappa_{\text{R}} = 0.2(1+X) \text{ cm}^2 \text{ g}^{-1}$ , where  $X$  is the hydrogen abundance.

Tabular values of opacity ([Iglesias & Rogers 1993, 1996](#); [Ferguson et al. 2005](#)) and EoS ([Rogers & Nayfonov 2002](#)) are obtained by interpolation using the kap and eos modules of the MESA code ([Paxton et al. 2011](#)). Notice that different chemical composition can be set if tabular opacity is used (see Sect. 5.2 below).

Opacity dependence on the temperature for a typical value of density  $\rho$  in a disc is shown in Fig. 1. Figure 2 shows differences between the analytical and tabular opacities described above.

## 2.3 Boundary conditions

We assume that at the surface of the disc the temperature is equal to the effective temperature

$$T_{\text{eff}} \equiv \left( \frac{Q_0}{\sigma_{\text{SB}}} \right)^{1/4} \quad (13)$$

and we use the grey Eddington approximation:

$$T = T_{\text{eff}} \left( \frac{1}{2} + \frac{3}{4}\tau \right)^{1/4}, \quad (14)$$

where  $\tau$  is the optical depth measured from outside inward to the disc symmetry plane. Thus we have boundary conditions on the temperature and flux:

$$T(z_0) = T(\tau = 2/3) = T_{\text{eff}}. \quad (15)$$

and

$$Q(z_0) = Q_0 \equiv Q_{\text{vis}}(z_0) = \frac{3}{8\pi} \frac{F\omega_{\text{K}}}{r^2}, \quad (16)$$

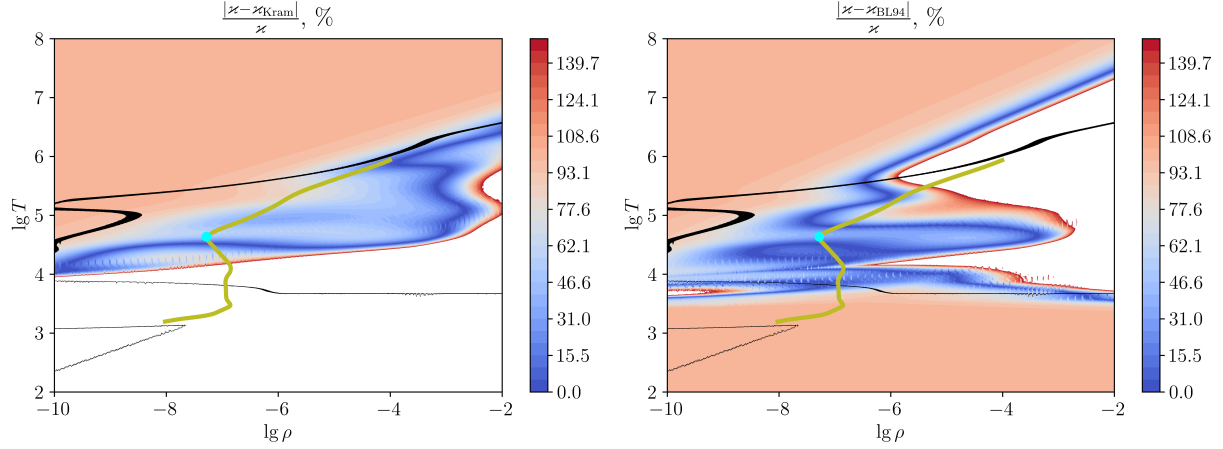


**Figure 2.** Shown are relative uncertainties between analytical approximations of opacity compared to tabular opacity values, obtained from MESA, as functions of density and temperature. Colour indicates the uncertainty in percents. In white regions the uncertainty is larger than 150%. The left panel shows the uncertainty relative to the Kramers opacity law, and the right one, to the approximations by Bell & Lin (1994) (see Sect. 2.2 for details). Black curve shows the range of  $\rho$  and  $T$ , where the electron scattering  $\kappa_T$  and absorption  $\kappa_{\text{ff}}$  opacity coefficients are equal. The olive curve shows the  $\rho - T$  relation for disc around  $M = 10 M_{\odot}$ , turbulent parameter  $\alpha = 0.1$  and accretion rate  $\dot{M} = 10^{18} \text{g s}^{-1}$ , corresponding to Fig. 4 below; the dot on the curve indicates the parameters at the outer hot zone radius.

where the viscous torque  $F = 2\pi r^2 W_r \varphi$ , and  $W_r \varphi \equiv \int_{-z_0}^{z_0} w_r \varphi dz$  is the integrated viscous stress. In a quasi-stationary accretion disc the viscous torque can be derived from the angular momentum conservation and is as follows:

$$F = \dot{M} h \left( 1 - \sqrt{\frac{r_{\text{in}}}{r}} \right) + F_{\text{in}}, \quad (17)$$

where  $h = \sqrt{GM r}$  is the specific angular momentum and  $F_{\text{in}}$  is the viscous torque at the inner radius  $r_{\text{in}}$  (see e.g. Shakura et al. 2018). Further we will assume that  $W_r \varphi$  is zero at the inner radius  $r_{\text{in}}$ , therefore  $F_{\text{in}} = 0$ . Generally, arbitrary torque  $F(r)$  can be set in the code.

To obtain the boundary condition for pressure, we write equation of hydrostatic equilibrium (2) in the photosphere:

$$\frac{dP}{d\tau} = \frac{\omega_K^2 z}{\kappa_R}, \quad (18)$$

where the optical depth  $\tau$ :

$$d\tau = -\kappa_R \rho dz, \quad (19)$$

so that the optical depth increases from the surface to symmetry plane. Integrating equation (18) gives:

$$P(z_0) = P' = \int_0^{2/3} \frac{\omega_K^2 z_0}{\kappa_R(P, T(\tau))} d\tau, \quad (20)$$

where (14) can be substituted. For analytical opacity, the integral can be taken analytically (Ketsaris & Shakura 1998). Notice that in the photosphere  $z$  coordinate practically does not change and equals to  $z_0$ .

The column density  $\Sigma$ , like optical depth, grows from  $z_0$  towards the disc symmetry plane:

$$\Sigma(z_0) = 0. \quad (21)$$

Note that this column density does not include the density of layers with  $\tau < 2/3$ .

The half-thickness of the disc  $z_0$  is a free parameter of the system. Thus, to solve the system one has to set additional boundary condition at the symmetry plane of the disc ( $z = 0$ ):

$$Q(0) = 0, \quad (22)$$

which follows from the symmetry of the problem.

## 2.4 Irradiation by central X-ray source

X-ray irradiation by the central accreting object (e.g., a neutron star) or by central parts of the accretion disc can be another source of heating in the disc. This heating can even exceed the viscous heating at large radii.

The effect of the incident radiation depends, naturally, on its spectrum. Soft X-rays are absorbed relatively high in the disc atmosphere and heat up the chromosphere-like layer, while photons  $> 3 \text{keV}$  can penetrate deep (Suleimanov et al. 1999). If they are absorbed in the layers below disc's photosphere (where the optical depth for its own emission  $\tau \sim 2/3$ ), X-ray photons are thermalized: their energy is contributed to the flux outgoing from the photosphere.

For irradiated discs the surface temperature rises in presence of irradiation, and the new boundary condition is

$$T^4(z_0) = T_{\text{vis}}^4 + T_{\text{irr}}^4, \quad (23)$$

where irradiation temperature  $T_{\text{irr}}$  measures the additional heating by X-rays. It will be defined differently in the two methods below. Note that for irradiated discs we rename the effective temperature (13) as viscous temperature

$$T_{\text{vis}} \equiv \left( \frac{Q_0}{\sigma_{\text{SB}}} \right)^{1/4}, \quad (24)$$

emphasizing its association with the viscous energy flux in contrast with irradiation temperature  $T_{\text{irr}}$ .

As we do not calculate an irradiated atmosphere model, we cannot calculate integral (20). Instead, following Tuchman et al. (1990) and Hameury et al. (1998), we assume that both the Rosseland opacity and  $z$  are constant in the photosphere and take value of pressure evaluated at  $\tau = 2/3$ :

$$P(z_0) = P' = \frac{2}{3} \frac{\omega_K^2 z_0}{\kappa_R(P', T(z_0))}. \quad (25)$$

We use two ways to include irradiation into calculation of the vertical structure. In the first method, only boundary conditions are

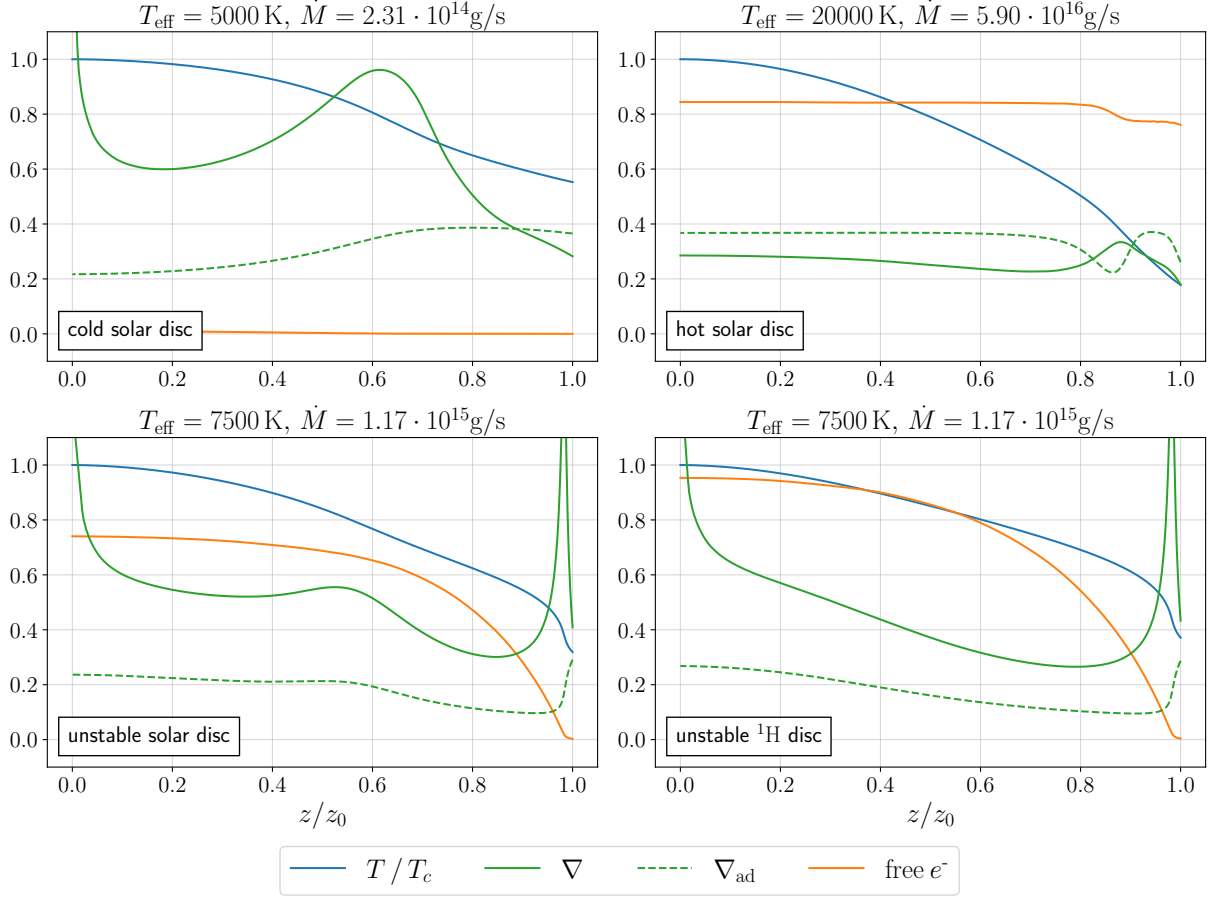


**Figure 3.** Disc vertical structure for  $M = 10 M_{\odot}$ ,  $\alpha = 0.1$ ,  $r = 10^{10}$  cm and tabular opacity for different accretion rates  $\dot{M}$  and effective temperatures  $T_{\text{eff}}$ . Shown are normalized temperature  $T/T_c$ , actual temperature gradient  $\nabla$ , adiabatic gradient  $\nabla_{\text{ad}}$ , and mean number of free electrons per nucleon. Upper panels are calculated for cold ( $T_{\text{eff}} = 5000$  K) and hot ( $T_{\text{eff}} = 20000$  K) disc states with solar composition. Lower panels are calculated for unstable disc states with solar and hydrogen composition. There is no convection in the hot disc ( $\nabla_{\text{rad}} < \nabla_{\text{ad}}$ ), while the disc in cold neutral and unstable states is convective.

changed (Tuchman et al. 1990; Dubus et al. 1999). In the second one, the equations themselves are altered too (e.g. Mescheryakov et al. 2011).

#### 2.4.1 (i) First method

In the first method, the boundary conditions on the temperature and pressure become (23) and (25); other boundary conditions as well as structure equations do not change. This roughly corresponds to all the heating taking place at the photosphere level.

Irradiation temperature  $T_{\text{irr}}$  can be expressed in terms of irradiation constant  $C_{\text{irr}}$ :

$$T_{\text{irr}}^4 = C_{\text{irr}} \frac{L_X}{4\pi\sigma_{\text{SB}}r^2}, \quad (26)$$

where  $L_X = \eta\dot{M}c^2$  is the X-ray luminosity of the central source.

#### 2.4.2 (ii) Second method

In the second method the X-ray radiation with arbitrary spectrum  $F_X^{\nu}(\nu)$  penetrates into the disc and affects distributions of the energy flux  $Q(z)$  and temperature  $T(z)$ . In the disc the additional source of

heating appears, so that Eq. (4) changes to the following form:

$$\frac{dQ}{dz} = \frac{d(Q_{\text{vis}} + Q_{\text{irr}})}{dz} = \frac{3}{2}\omega_K\alpha P + \varepsilon, \quad (27)$$

where  $\varepsilon$  and  $Q_{\text{irr}}$  are the local heating rate of the disc through X-ray photons and the corresponding vertical energy flux. They are calculated from the analytical solution of radiation transfer equation for X-ray photons and by integrating over the entire spectrum (see equations (17)–(21) in Mescheryakov et al. (2011) and Appendix B). Accordingly, the boundary condition on flux is changed:

$$Q(z_0) = Q_0 + Q_{\text{irr}}(z_0), \quad (28)$$

see (B5).

The temperature and pressure boundary conditions are still (23) and (25), respectively. Equations (13) and (16) are applicable as well.

While in the previous method the irradiation temperature or irradiation constant can be an input parameter, now  $T_{\text{irr}}$  is calculated from obtained flux  $Q_{\text{irr}}$  at the photosphere level:

$$\sigma_{\text{SB}}T_{\text{irr}}^4 = Q_{\text{irr}}(z_0). \quad (29)$$

The system has two free parameters:  $z_0$  and the surface density of the disc  $\Sigma_0$ . Therefore, the code solves a two-parameter optimization problem and finds  $(z_0, \Sigma_0)$ . Contrary to the previous method, where the surface density of the disc is obtained on solving the equations,

now one has to set the additional boundary condition, complementary to (22):

$$\Sigma(z=0) = \Sigma_0. \quad (30)$$

We assume that X-ray radiation comes from the point-like central object, whose flux at distance  $r$  is:

$$F_X^{\nu}(r) = \frac{L_X}{4\pi r^2} S(\nu), \quad (31)$$

where  $S(\nu)$  is the spectrum of incident X-ray flux, and  $L_X$  is the X-ray luminosity of central source. Both  $S(\nu)$  and  $L_X$  can be set by user in the code (see Appendix D).

### 3 VERTICAL STRUCTURE

We have developed the Python 3 code that solves equations presented above. Code is open-source and available from GitHub<sup>2</sup>. Appendix D contains a description of the code, while the numerical details of the calculation scheme are given in Appendix E.

Fig. 3 presents examples of the vertical structure for different effective temperatures (which are related with accretion rate) at fixed radius  $r = 10^{10}$  cm for a case without external irradiation. Shown are temperature distribution, adiabatic and actual temperature gradients, and the mean number of free electrons per nucleon free  $e^- \equiv 1/\mu_e$ . The latter can change from 0 in neutral matter to  $(1+X)/2$  in fully ionized matter, where  $X$  is the hydrogen abundance.

Note that the panels of Fig. 3 correspond to different disc states. The upper panels represent stable disc (in hot and cold state), while lower panels show unstable disc with different chemical composition (solar and pure hydrogen). The latter solutions lie on the negative branch on the S-curve, see Sect. 5 and Fig. 10. The unstable state is related to ionization of hydrogen: while the cold disc is neutral (free  $e^- \approx 0$ ) and hot disc is fully ionized (free  $e^- \approx 0.85$ ), ionization of unstable disc changes along  $z$  between these two limits.

The disc in cold and unstable state is convective ( $\nabla_{\text{rad}} > \nabla_{\text{ad}}$  along the  $z$  coordinate), while there is no convection in the hot disc (except for a thin layer near the surface). This happens regardless of the chemical composition: the pure helium disc behaves similarly. The main difference is that instability in helium disc is related to the partial ionization of helium, therefore the temperature of unstable disc ( $T_{\text{eff}} \sim 15\,000$  K) is higher than in that in pure hydrogen or solar disc ( $T_{\text{eff}} \sim 7\,000$  K). The corresponding S-curves are presented in Sect. 5.2, see Fig. 12 and 13.

Examples of vertical structure for irradiated disc can be found in Appendix C. The influence of external irradiation depends on the relation between the irradiation and viscous temperatures and on the total optical depth of the disc  $\tau_0$ . If  $Q_{\text{irr}}/Q_{\text{vis}} < \tau_0$ , irradiation hardly affects the vertical structure, if there is no convection (see Fig. C1).

Notice that, if an un-irradiated disc is convective, external irradiation reduces the role of convection and may completely stop it, which leads to rise of the central temperature; that is, irradiation may affect a convective disc very strongly (see also Tuchman et al. 1990).

We have checked the consistency of the code with results of some previous works. For analytic opacities the obtained vertical structure of un-irradiated disc agrees with results by Ketsaris & Shakura (1998) (see Tavleev et al. 2019, 2022). The irradiated disc structure agrees with results by Mescheryakov et al. (2011) and that by Dubus et al. (1999); Tuchman et al. (1990), for corresponding methods.

### 4 RADIAL STRUCTURE

Standard model of the disc accretion defines three radial zones (Shakura & Sunyaev 1973). In zone A, the radiation pressure is greater than the gas pressure, and opacity is determined by scattering. In zone B, the gas pressure is greater than the radiation pressure, but opacity is still determined by scattering. Finally, in zone C, opacity is determined by the absorption processes, and gas pressure is much greater than the radiation pressure.

Suleimanov et al. (2007) demonstrated that analytic radial dependencies of disc parameters could be written more accurately if solutions of vertical structure are taken into account for analytical opacity coefficient and EoS. This approach relies on the method of vertical-structure calculation by Ketsaris & Shakura (1998).

Ketsaris & Shakura (1998) introduce dimensionless  $\Pi$ -parameters:

$$\begin{aligned} \Pi_1 &\equiv \frac{\omega_K^2 z_0^2 \rho_c}{P_c}, & \Pi_2 &\equiv \frac{\Sigma_0}{2z_0 \rho_c}, \\ \Pi_3 &\equiv \frac{3}{4} \frac{\alpha \omega_K P_c \Sigma_0}{\rho_c Q_0}, & \Pi_4 &\equiv \frac{3}{32} \left( \frac{T_{\text{eff}}}{T_c} \right)^4 \Sigma_0 \kappa_c. \end{aligned} \quad (32)$$

Here  $P_c, T_c, \rho_c$  are the gas pressure, temperature and bulk density in the symmetry plane. Values of  $\Pi$ -parameters are found on solving the vertical structure. Ketsaris & Shakura (1998) use the Kramers formula in the regions, where absorption prevails the scattering, and Thomson scattering coefficient for hotter regions. Malanchev et al. (2017) generalize these solutions for an arbitrary opacity power law.

Knowing  $\Pi$ -values one can obtain from (32) analytical formulas for the radial distribution of  $z_0/r, \Sigma_0, T_c, \rho_c$ . It was done for Kramers and Thomson opacity in Suleimanov et al. (2007), see also Shakura et al. (2018). As can be seen in Fig. 2, near the outer boundary of the hot disc (the cyan dot on the olive curve) the opacity approximation  $\kappa_R \sim \rho T^{-5/2}$  fits on average better the actual disc opacity, than the Kramers law ( $\kappa_R \sim \rho T^{-7/2}$ ) does, while opacity in the inner parts of the disc (with higher temperatures) are better approximated by the Kramers law.

Let us substitute the EoS of ideal gas in (32) along with the opacity approximation formula obtained by Bell & Lin (1994) for hot disc regions, where opacity is determined by free-free and bound-free transitions. We obtain:

$$z_0/r = 0.0207 m^{-13/36} \alpha^{-1/9} r_{10}^{1/12} \dot{M}_{17}^{1/6} f(r)^{1/6} \left( \frac{\mu}{0.6} \right)^{-13/36} \left( \frac{\kappa_0}{\kappa_0^*} \right)^{1/18} \Pi_z, \quad (33)$$

$$\Sigma_0 = 32 m^{2/9} \alpha^{-7/9} r_{10}^{-2/3} \dot{M}_{17}^{2/3} f(r)^{2/3} \left( \frac{\mu}{0.6} \right)^{13/18} \left( \frac{\kappa_0}{\kappa_0^*} \right)^{-1/9} \Pi_{\Sigma} [\text{g cm}^{-2}], \quad (34)$$

$$\rho_c = 7.8 \cdot 10^{-8} m^{7/12} \alpha^{-2/3} r_{10}^{-7/4} \dot{M}_{17}^{1/2} f(r)^{1/2} \left( \frac{\mu}{0.6} \right)^{13/12} \left( \frac{\kappa_0}{\kappa_0^*} \right)^{-1/6} \Pi_{\rho} [\text{g cm}^{-3}], \quad (35)$$

$$T_c = 4.1 \cdot 10^4 m^{5/18} \alpha^{-2/9} r_{10}^{-5/6} \dot{M}_{17}^{1/3} f(r)^{1/3} \left( \frac{\mu}{0.6} \right)^{5/18} \left( \frac{\kappa_0}{\kappa_0^*} \right)^{1/9} \Pi_T [\text{K}]. \quad (36)$$

<sup>2</sup> <https://github.com/AndreyTavleev/DiscVerSt>

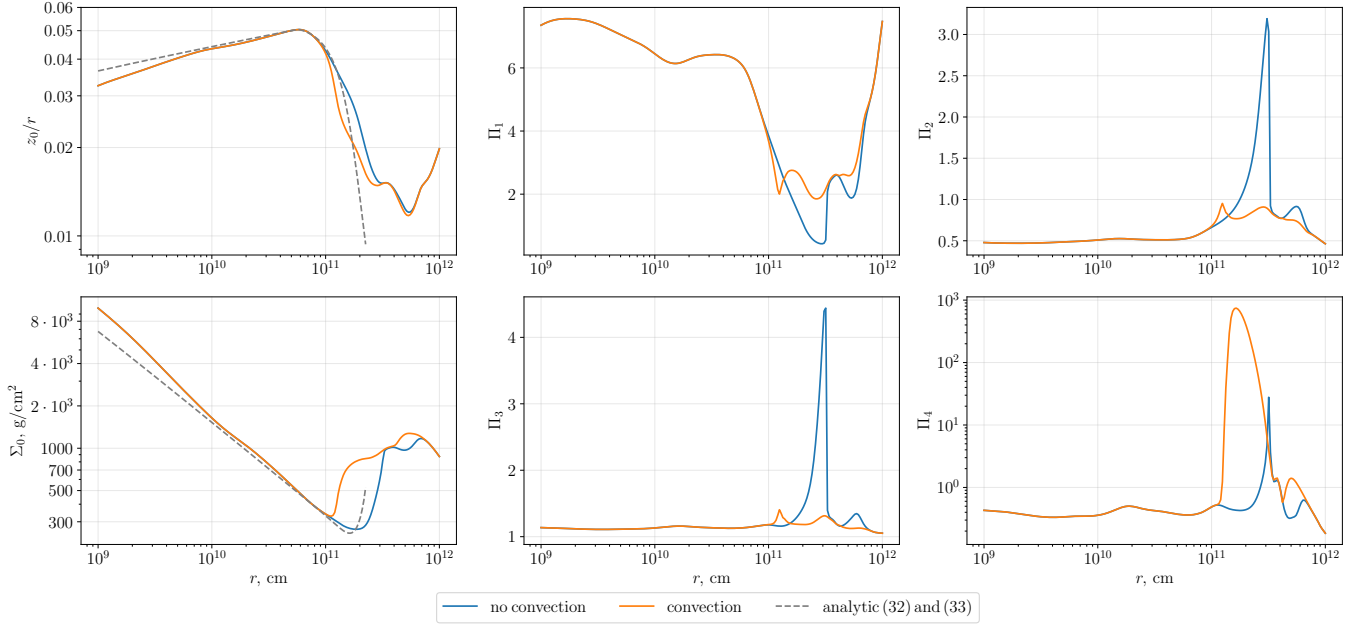


**Figure 4.** Radial structure of disc with  $M = 10 M_{\odot}$ ,  $\alpha = 0.1$ ,  $\dot{M} = 10^{18} \text{g s}^{-1}$ , with and without convection together with theoretical approximations (33–34). Shown are the semi-thickness of disc  $z_0/r$  and surface density  $\Sigma_0$ . It is clearly seen that convection thins the unstable part of the disc. Also shown are the  $\Pi$  parameters (32).

Here:

$$m \equiv \frac{M}{M_{\odot}}, \quad \dot{M}_{17} \equiv \frac{\dot{M}}{10^{17} \text{g s}^{-1}}, \quad r_{10} \equiv \frac{r}{10^{10} \text{cm}}, \quad (37)$$

$$\kappa_0^* \equiv 1.5 \cdot 10^{20} \text{cm}^5 \text{g}^{-2} \text{K}^{5/2}, \quad f(r) \equiv \frac{F}{\dot{M}h} = 1 - \sqrt{\frac{r_{\text{in}}}{r}}.$$

Dimensionless parameters  $\Pi_z, \Pi_{\Sigma}, \Pi_{\rho}, \Pi_T$  are almost constant in optically thick discs ( $\tau \gtrsim 10^4$ , see e.g., Suleimanov et al. (2007)) and are as follows:

$$\begin{aligned} \Pi_z &= \Pi_1^{17/36} \Pi_2^{-1/18} \Pi_3^{1/9} \Pi_4^{-1/18} \approx 2.744, \\ \Pi_{\Sigma} &= \Pi_1^{1/18} \Pi_2^{1/9} \Pi_3^{7/9} \Pi_4^{1/9} \approx 1.049, \\ \Pi_{\rho} &= \Pi_1^{-5/12} \Pi_2^{-5/6} \Pi_3^{2/3} \Pi_4^{1/6} \approx 0.771, \\ \Pi_T &= \Pi_1^{-1/18} \Pi_2^{-1/9} \Pi_3^{2/9} \Pi_4^{-1/9} \approx 1.095. \end{aligned} \quad (38)$$

Figure 4 presents the radial structure of solar disc with and without convection together with analytical approximations (33–34), which are in good agreement with calculations in the stable region. Notice that actual values of  $\Pi$  are substituted into (33–34) and they are far from being constant in the zone with partial ionization, explaining non-monotonic behaviour of the dashed curve.

It should be kept in mind that some intervals of the radial dependencies in Fig. 4 correspond to thermally-unstable solutions of the vertical structure, these intervals manifest themselves by sharp positive slope of the surface density radial profile. This means that the depicted radial structure for constant  $\dot{M}$  for all depicted radii could not exist in reality during times longer than the local thermal time. At the same time, the depicted radial dependencies in the hot ionized stable zone (solid lines, where the surface density monotonically drops from the centre), and Eqs. (33)–(36) (in the outermost parts of the stable hot zone) describe satisfactory the quasi-stationary structure of corresponding parts of an evolving disc. Quasi-stationary means

on a time-scale less than the viscous time calculated at the outer radius of the ionized disc.

Notice that account of the convection “shifts” the instability region to the smaller radii.

#### 4.1 Checking the disc zones

Using expressions (33–36), one can estimate the boundary  $R_{BC}$  between B zone and C zone from the equality of electron scattering  $\kappa_T$  and absorption  $\kappa_{\text{ff}} = \kappa_0 \rho_c T_c^{-5/2}$  opacity coefficients. However, that gives the implausible value  $R_{BC} \sim 7 \cdot 10^4 \text{cm}$ , which is related to the fact that for high-temperature plasma, when the value of opacity is around the Thomson scattering, the Bell-Lin approximation of opacity is very poor, see Fig. 2. One can see that the Kramers law better approximates the opacity for big densities and temperatures, so to find the boundary  $R_{BC}$  one should use it, which gives (Suleimanov et al. 2007):

$$R_{BC, \text{Kramers}} \approx 5 \cdot 10^7 m^{1/3} \dot{M}_{17}^{2/3} f(r)^{2/3} \left(\frac{\mu}{0.6}\right)^{-1/3} \left(\frac{\kappa_0}{\kappa_0^*}\right)^{-2/3} \left(\frac{\kappa_T}{\kappa_T^*}\right)^{4/3} [\text{cm}], \quad (39)$$

where  $\kappa_T^* = 0.335 \text{cm}^2/\text{g}$ , corresponding to the fully ionized hydrogen, and  $\kappa_0^* \equiv 5 \cdot 10^{24} \text{cm}^5 \text{g}^{-2} \text{K}^{7/2}$ , as in Kramers opacity law. Boundary between A zone and B zone,  $R_{AB}$ , can be obtained from the equality of  $P_{\text{rad}} = aT^4/3$  and  $P_{\text{gas}}$ , while opacity is determined by scattering:

$$R_{AB} \approx 10^7 m^{1/3} \alpha^{2/21} \dot{M}_{17}^{16/21} f(r)^{16/21} \left(\frac{\mu}{0.6}\right)^{8/21} \left(\frac{\kappa_T}{\kappa_T^*}\right)^{6/7} [\text{cm}]. \quad (40)$$

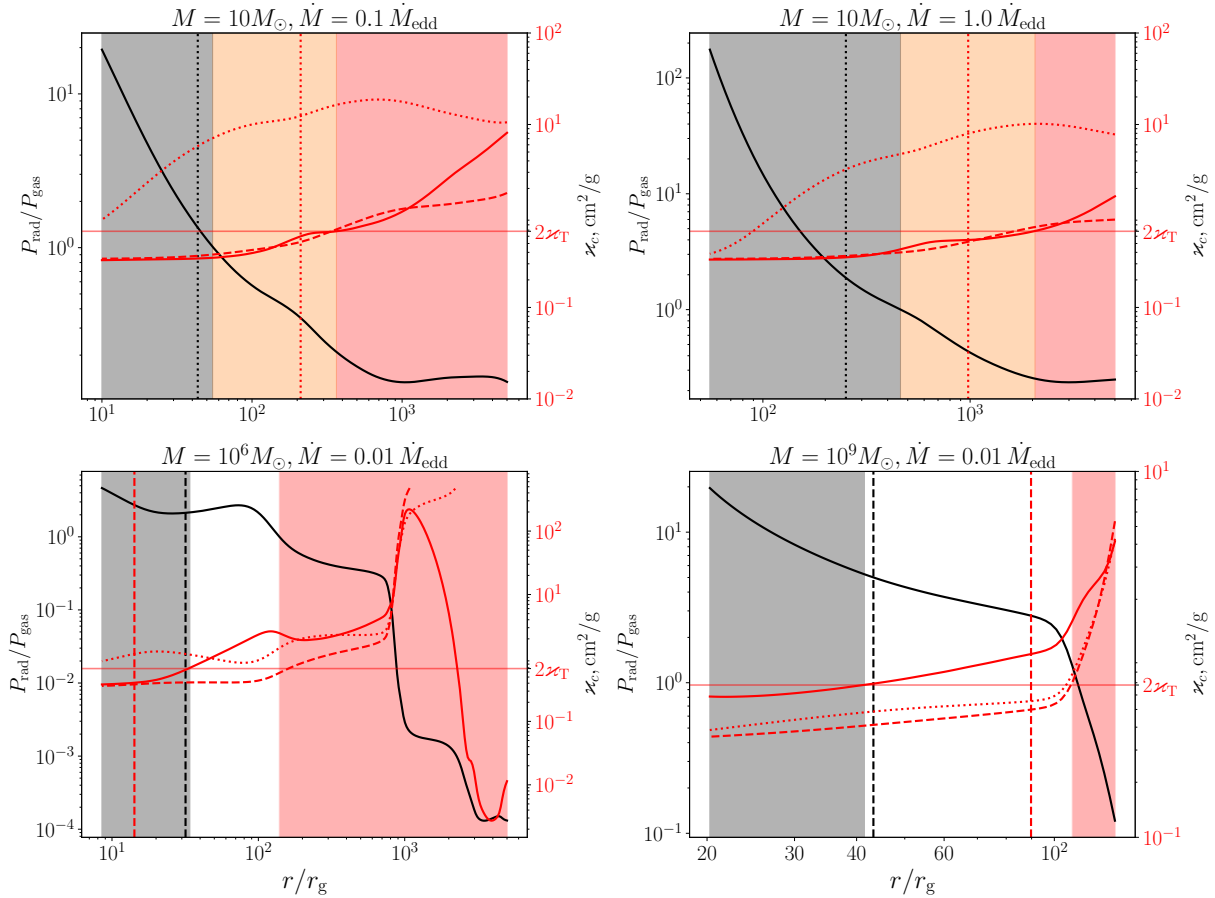


**Figure 5.** Disc zones for different masses of accretors. Black curve shows the radiation to gas pressure ratio at the symmetry plane (on the left Y-axis), which is greater than 1 in the grey region. Red solid curve shows the total Rosseland opacity (on the right Y-axis), which is greater than  $2\alpha_T$  in the red region. Other red curves show analytic opacity: via Kramers law (dashed) and Bell & Lin (1994) expression (dotted) for absorption and the Thomson electron scattering. White region in the right bottom panel corresponds to zone B\*, see description in the text. Description of the vertical lines, which are the analytic estimates of zone boundaries, is given in the text. Turbulence parameter  $\alpha = 0.1$ . Note that the outer radius of the disc around  $10^9 M_\odot$  is determined by self-gravity of the disc, that is, at the outer boundary of the disc, the self-gravity balances the attraction to the central object (i.e.  $2\pi G\Sigma/\omega_K^2 z_0 = 1$ ).

Figure 5 shows radiation pressure to gas pressure ratio  $P_{\text{rad}}/P_{\text{gas}}$  and tabular opacity  $\kappa_c$  at the symmetry plane of the disc (solid lines). Using these values, disc zones are distinguished: they are shown with colored backgrounds. In the grey region, visible in the upper panels of Fig. 5, the radiation pressure prevails in the disc and opacity is mainly due to scattering, namely, the total Rosseland opacity is less than  $2\alpha_T$  – this interval of radii corresponds to zone A. In the red region, the situation is the opposite, which corresponds to C zone of the disc. The intermediate B zone, seen for  $10 M_\odot$ , is shown in peach. Its width decreases with increasing  $M$ .

The dotted black and red vertical lines, shown for  $10 M_\odot$  in Fig. 5, are the analytic estimates of zone boundaries (40) and (39), respectively. One can see that for central objects of stellar masses and for accretion rates about  $0.1 - 1 \dot{M}_{\text{edd}}$ , the analytical estimate  $R_{AB}$  (40) and the ‘actual’ boundary of zone A are in good agreement. Concerning (39), one can see that the opacity for disc around stellar-mass objects near the B/C transition is indeed better approximated with the Kramers law (dashed red curve) than with the Bell & Lin (1994) opacity expression (dotted red curve).

For supermassive black holes, inwards from zone C there could be a zone, shown with white background for  $10^6 M_\odot$  and  $10^9 M_\odot$ , where the radiation pressure prevails while the main contribution to

opacity is from free-free and bound-free transitions. We coin this zone B\*, following Burderi et al. (1998). They estimate analytically the B\* zone boundaries, namely  $R_{AB^*}$  and  $R_{B^*C}$ , which are shown, respectively, by black and red vertical dashed lines in the bottom panels of Fig. 5. Unfortunately, the analytical estimates poorly locate zone B\*, possibly, due to averaging of vertical structure or analytic opacities. For disc around  $10^6 M_\odot$  the analytical estimates even do not indicate the presence of zone B\*. Thus, one is advised to describe the disc structure around a supermassive black hole using the numerical results, such as provided by our code.

## 4.2 Irradiated disc

Figure 6 presents radial profiles of the vertical height  $z_0/r$ , surface density  $\Sigma_0$ , mid-plane temperature  $T_c$ , temperature at the photosphere  $T_{\text{ph}}$ , irradiation temperature  $T_{\text{irr}}$  and irradiation constant  $C_{\text{irr}}$  for un-irradiated and irradiated disc. Unless indicated otherwise, for the central X-ray luminosity  $L_X = \eta \dot{M} c^2$  we assume accretion efficiency  $\eta = 0.1$ . Irradiation is taken into account by two methods (see Sect. 2.4: with scheme (i) for two values of  $C_{\text{irr}}$  (the dark and light green lines) and with advanced scheme (ii) for different X-ray luminosities (the blue, orange, and magenta lines).

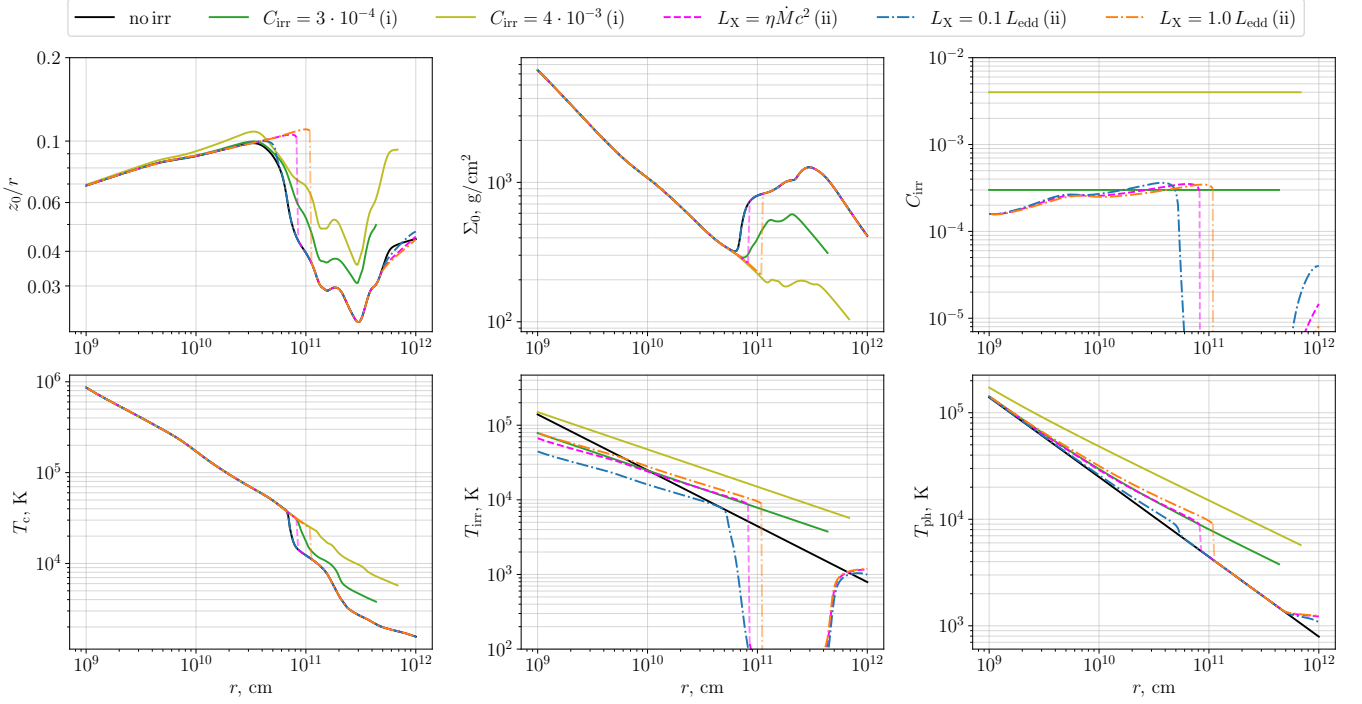


**Figure 6.** Radial profiles of the vertical height  $z_0/r$ , surface density  $\Sigma_0$ , mid-plane temperature  $T_c$ , temperature at the photosphere  $T_{\text{ph}}$ , irradiation temperature  $T_{\text{irr}}$  and irradiation constant  $C_{\text{irr}}$  for un-irradiated disc and irradiated disc with irradiation scheme (i) (see Sect. 2.4) for two  $C_{\text{irr}}$ , and with advanced scheme (ii) for different X-ray luminosities. Mass of central object  $M = 1.4 M_{\odot}$ ,  $\alpha = 0.1$ ,  $\dot{M} = 10^{18} \text{ g s}^{-1} \approx 0.5 \dot{M}_{\text{edd}}$ . The black line in lower figures shows the viscous temperature  $T_{\text{vis}}$ .

In scheme (ii), for spectrum of incident X-rays in expression (31) we take:

$$S(\nu) \propto \left( \frac{E}{kT_{\text{sp}}} \right)^{-0.4} \exp\left( -\frac{E}{kT_{\text{sp}}} \right) \quad (41)$$

in the range 1 – 10 keV, with  $T_{\text{sp}} = 8 \text{ keV}$  (Mescheryakov et al. 2011). Note that spectrum  $S(\nu)$  is the parameter of the code and can be set manually (see Appendix D). The incident angle of external irradiation is assumed to be

$$\cos \theta_0 \approx \frac{dz_0}{dr} - \frac{z_0}{r} = \frac{z_0}{r} \left( \frac{d \ln z_0}{d \ln r} - 1 \right) = \frac{1}{12} \frac{z_0}{r}, \quad (42)$$

following the analytical approximation (33) for  $z_0/r$ , which is quite satisfactory at the outer disc (see panel  $z_0/r$  in Fig. 4).

The last formula could introduce a limitation to scheme (ii) since it does not take into account the disc profile self-consistently. For  $\dot{M} = \text{const}$  the profile of  $z_0/r$  is formally negative beyond the hot zone (see Fig. 4 or 6) and the outer radii are shadowed. This means that the profile of un-irradiated disc (the black solid line) should apply for shadowed zones. If one looks closer, it is evident that scheme (ii) provides virtually the same solution as the un-irradiated disc model in the shadowed regions. This happens because the calculated in (ii) value of  $C_{\text{irr}}$  drops dramatically.

On the other hand, the height where the X-rays are effectively intercepted may differ from  $z_0$  remarkably. This can be due to scattering above the disc (Suleimanov et al. 2007; Mescheryakov et al. 2011). This can be taken into account by changing relation (42), see Appendix D.

#### 4.2.1 Comparing results of methods for irradiated disc

In confirmation with results of previous works (e.g., Dubus et al. 1999), strong irradiation keeps the disc in the hot state at farther distances, comparing to the case without irradiation. We find that irradiation method affects the hot disc size only very slightly. For comparable values of  $Q_{\text{irr}}$ , cf. the dark green and magenta lines in Fig. 6, the hot disc has very similar radial extension, which is seen in the panel for  $\Sigma$  as a location where the surface density starts to rise going outwards.

Furthermore, stabilization of the disc’s vertical structure by irradiation with  $T_{\text{irr}} \gtrsim 10^4 \text{ K}$ , previously found by Tuchman et al. (1990); Dubus et al. (1999), occurs in our calculations by either irradiation method. The temperature of the stability loss, which is actually  $\lesssim 9000 \text{ K}$ , is investigated by us in detail in section 6.

At the same time, it should be noted that the method (i) implies a disc structure that is not self-consistent. For example, in Fig. 6 the self-shadowing of the disc at distances farther than  $\sim 4 \cdot 10^{10} \text{ cm}$  contradicts the notion of a constant irradiation parameter. Moreover, the method of irradiation (ii) allows one to calculate  $C_{\text{irr}}$ , whereas the method (i) uses it as an input parameter.

#### 4.2.2 Value of $C_{\text{irr}}$

The irradiation parameter  $C_{\text{irr}}$  and irradiation temperature  $T_{\text{irr}}$  for advanced scheme (ii), also shown in Fig. 6, can be calculated from flux  $Q_{\text{irr}}$  supplied by thermalized external emission (see (29) and (B8)). One can see that they drop dramatically in the region where  $T_{\text{irr}} < 9000 \text{ K}$ . On comparing the curves for  $C_{\text{irr}}$  with the behaviour of disc semi-thickness, we infer that the drop of  $C_{\text{irr}}$  is not due to

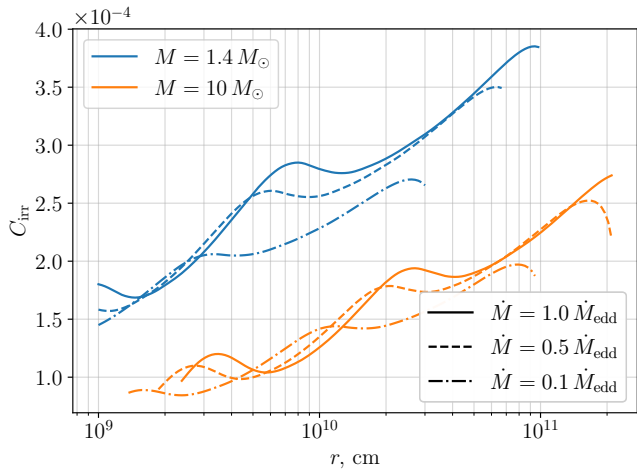


**Figure 7.** Radial profile of irradiation parameter  $C_{\text{irr}}$  for two masses ( $M = 1.4, 10 M_{\odot}$ ) and three accretion rates ( $\dot{M} = 0.1, 0.5, 1 \dot{M}_{\text{edd}}$ ),  $\alpha = 0.1$ .

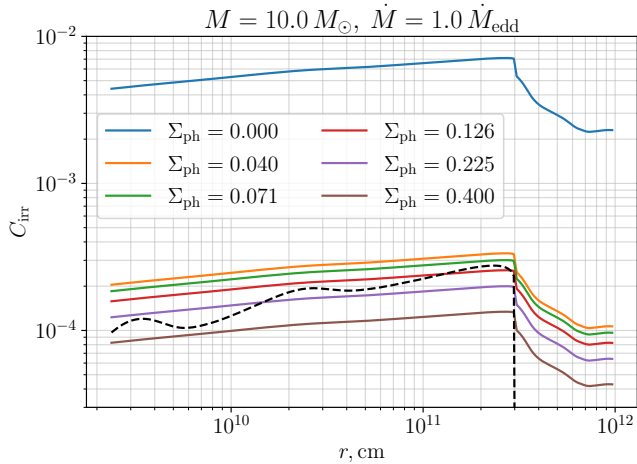


**Figure 8.** Radial profile of  $C_{\text{irr}}$ , when the column density of the photosphere layer above the disc surface  $\Sigma_{\text{ph}} = \text{const}$  (coloured solid lines) in contrast with realistic  $C_{\text{irr}}$  profile (the black dashed line). System parameters are  $M = 10 M_{\odot}$ ,  $\dot{M} = 1 \dot{M}_{\text{edd}}$ ,  $\alpha = 0.1$ . The legends give the photosphere column density in  $\text{g cm}^{-2}$ . Drop of  $C_{\text{irr}}$  on the left occurs in the zone of the disc where the vertical structure is unstable.

a purely geometrical effect, since the cosine between incident rays and normal to the disc surface, which is set proportional to  $z_0/r$  according to (42), decreases by only a few times. We deduce that the drop happens due to strong absorption of X-ray photons above the disc photosphere, so that the external irradiation hardly affects the disc vertical structure. This increased absorption is driven by a very high column density in the photosphere of the outer part of a disc<sup>3</sup> (see the dashed line in Fig. 8 below).

According to expression (B2) and (B9),  $C_{\text{irr}}$  value depends on the X-ray spectrum, angle of incident rays and optical depth to X-rays above the level where the optical flux  $\sigma_{\text{SB}} T_{\text{vis}}^4$  is formed (it is  $\tau = 2/3$

<sup>3</sup> The high photosphere density, in its turn, is an artefact of the formal request that  $\dot{M} = \text{const}$  at all radii. If, alternatively,  $\Sigma_0$  is smooth,  $\dot{M}$  drops beyond the hot disc.

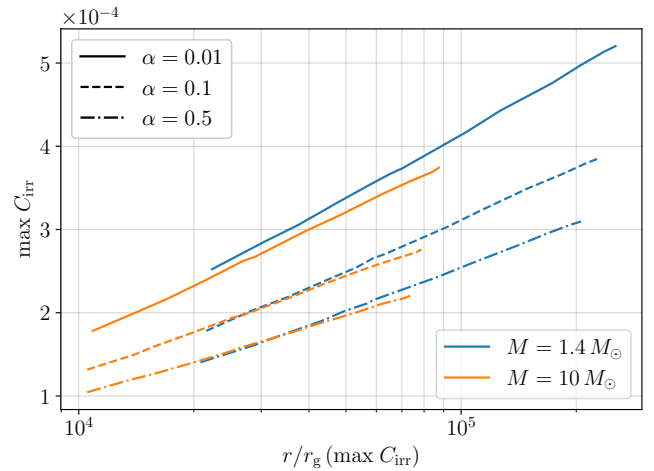


**Figure 9.** Maximum  $C_{\text{irr}}$  for accretion rates  $(10^{-2} - 1) \dot{M}_{\text{edd}}$ , as function of the radius (in Schwarzschild radius) for two central source masses (different colors) and three  $\alpha$ -parameters (different styles). Irradiation is taken into account by method (ii) and  $L_X = \eta \dot{M} c^2$ .

in our scheme). For a simplified case of single-frequency X-ray photons,  $\Sigma_{\text{ph}} = 0$  ( $\Sigma_{\text{ph}}$  is the column density of the photosphere layer above the disc surface) and total optical thickness of the disc  $\tau_0 \gg 1$  it can be shown analytically that  $C_{\text{irr}} = (1 - A) \cos \theta_0$ , where  $A$  is the frequency-dependent albedo (see Eq. (B10) and equation A39 in Mescheryakov et al. (2011)). This is in agreement with the previously proposed definition of  $C_{\text{irr}}$ , according to which, for a point-like source, the irradiation parameter can be written as (e.g., Suleimanov et al. 2007)

$$C_{\text{irr}} = (1 - A) \frac{z_0}{r} \left( \frac{d \ln z_0}{d \ln r} - 1 \right), \quad (43)$$

where  $1 - A$  is the fraction of incoming X-ray flux that is subject to thermalization.

Fig. 7 shows radial dependences of the irradiation parameter for different masses and accretion rates for the fixed spectrum (41). We stress that  $C_{\text{irr}}$  depends on the the upper boundary condition that defines  $\Sigma_{\text{ph}}$  and determines the pressure condition (25). The dependence  $\Sigma_{\text{ph}}(r)$  is what drives the radial ‘wiggles’ of  $C_{\text{irr}}$  in Fig. 7: fixing photosphere column density to a constant value provides much more smooth  $C_{\text{irr}}$  behaviour, see Fig. 8. As we have checked, the dependence on radius of the solid lines in Fig. 8 comes solely from the disc opening angle  $z_0(r)/r$ .

One could expect that  $C_{\text{irr}} \propto z_0/r$ . If albedo  $A$  in (43) is constant then a new parameter  $\tilde{C}_{\text{irr}}$  can be suggested via

$$C_{\text{irr}} = \tilde{C}_{\text{irr}} \frac{z_0}{r}, \quad (44)$$

see, e.g., Lipunova et al. (2022). Fig. B1 in the Appendix shows the radial profile of  $\tilde{C}_{\text{irr}}$ . Indeed the variability of  $\tilde{C}_{\text{irr}}$  with radius is less that that of  $C_{\text{irr}}$ . However,  $\tilde{C}_{\text{irr}}$  appears to depend on the accretion rate, which, possibly, is due to a nontrivial dependence of  $\Sigma_{\text{ph}}$  and  $A$  on  $\dot{M}$ . Auxiliary calculations have shown that, for varying value of the turbulent parameter  $\alpha$ , from 0.01 to 0.5, the value of  $\tilde{C}_{\text{irr}}$  changes by only about  $\pm 5\%$ . However, since the method of calculation of irradiated disc (ii) engages approximate boundary conditions, one should be cautious in the respect of relationship between the specific calculated values and reality.

Summarizing, values of  $C_{\text{irr}}$ , calculated by our code, are comparable or smaller than those suggested in previous works. For specific

X-ray spectrum, calculated irradiation parameter  $C_{\text{irr}}$  is in the range  $(1-5) \times 10^{-4}$  (Fig. 9). [Esin et al. \(2000\)](#) obtain  $C_{\text{irr}} \sim 0.004$  by analyzing the light curves of soft X-ray transient A0620-00 (1975), and  $C_{\text{irr}} \approx 0.0014$  for GRS 1124-68 (1991). Those values are consistent with estimate  $C_{\text{irr}} \sim (2-4) \times 10^{-3}$  found by ([de Jong et al. 1996](#)) for some Low-Mass X-ray Binaries. On the other hand, [Suleimanov et al. \(2008\)](#) for the same two transients obtain  $C_{\text{irr}} \sim 7 \times 10^{-4}$  and  $C_{\text{irr}} \sim 3 \times 10^{-4}$ , respectively. [Lipunova & Malanchev \(2017\)](#) estimate that  $C_{\text{irr}} \sim (3-6) \times 10^{-4}$  using optical data of 4U 1543-47 (outburst of 2002).

There is a physical reason of why our irradiation scheme provides the lower limit on  $C_{\text{irr}}$ . The present scheme involves neither additional heating of the disc by soft-X-rays-heated upper layers of the photosphere (above  $\tau = 2/3$ ) nor the increased X-ray flux due to scattering in even higher and hotter corona (see [Mescheryakov et al. 2011](#)).

## 5 S-CURVES

[Meyer & Meyer-Hofmeister \(1981\)](#) have established that dependencies  $F - \Sigma_0$  (S-curves) show the disc instability: the branch of the S-curve with a negative slope represents solutions to the vertical structure equations which are viscously unstable, i.e. oscillations have to develop during characteristic time of order of the viscous time. [Smak \(1982b, 1984\)](#) has showed that if the parameters of the disc at some radius lie on the viscous-unstable branch of the S-curve, then thermal instability also develops at this radius. Note that since the quasi-stationary discs has an unambiguous relation between  $F$ ,  $\dot{M}$  and  $T_{\text{eff}}$  (see Eqs. (13, 15–17)), the S-curve can be drawn also in coordinates  $\dot{M} - \Sigma_0$  and  $T_{\text{eff}} - \Sigma_0$ .

An example of an S-curve calculated by our code is shown in Fig. 10, the top left panel. Arrows shows schematically the direction of ring evolution when an outburst happens.

According to DIM, an outburst can be described in the following scenario ([Frank et al. 2002](#); [Done et al. 2007](#); [Kato et al. 2008](#)). Suppose, a cold neutral disc is fueled by gas flowing from a companion star. Presumably, the gas accumulates at some radii because the viscosity is not high enough to transfer the angular momentum efficiently when the gas is not hot enough and neutral. Starting from a state at a lower positive branch, between marks ‘a’ and ‘b’ on the Fig. 10, if the surface density increases at the particular radius, the critical value (right turn ‘b’) is eventually approached. During this relatively slow evolution the hydrogen is gradually more and more ionized (see the right bottom panel). When the temperature gets a bit higher and the hydrogen is substantially ionized (at mark ‘b’: more than  $\sim 50\%$  of full ionization at the symmetry plane of a disc), further temperature increase leads to a runaway heating until the free-free emission can balance the heating (mark ‘e’): the thermal instability develops.

Heating on the scale of the thermal time puts the disc somewhere on the upper stable branch (not exactly at the same surface density, as schematically shown). According to DIM ([Hameury et al. 1998](#); [Hameury 2020](#)), this transition is accompanied by increasing turbulent parameter  $\alpha$ , due to a change in the ionization state ([Smak 1984](#)). Actually, the change of the turbulent parameter, assumed in DIM models, is dictated by the need to produce outbursts of observed amplitude (see e.g., [Hameury et al. 2009](#)). Examples of S-curves calculated with different values of  $\alpha$  are presented in Figs. 12 and 13. Since the S-curve in Fig. 10 is plotted for a fixed value of  $\alpha$ , the arrows just indicate the direction of DIM evolution.

On the higher positive branch the viscous evolution of the disc

goes rapidly due to higher temperature (and likely higher  $\alpha$ ) and the mass evacuates the ring on its way towards the centre. Some matter comes from the outer radius but, on the whole, the evolution diminishes mass and density in the disc. Accordingly, the surface density decreases and, eventually, the ring reaches the left turn ‘e’ – the critical point beyond which no stable ‘hot’ solution is possible: the ring transits to neutral ‘cold state’ (again not exactly at the same surface density as the scheme shows).

Other panels in Fig. 10 show the dependence of the symmetry plane temperature on surface density, and the opacity and the mean number of free electrons per nucleon (free  $e^- \equiv 1/\mu_e$ ) on the temperature at different depths  $z$ . Ionization of hydrogen in the disc symmetry plane starts at a temperature of  $T_c \approx 10^4$  K. When free  $e^-$  reaches the value of  $\sim 0.4$ , the thermal instability begins. It ends when the disc is almost completely ionized (free  $e^-$  at the central plane is  $\sim 0.77$ ).

We have computed several thousand S-curves for  $\alpha$  from  $3 \cdot 10^{-4}$  to 0.7,  $M$  from  $1 M_\odot$  to  $20 M_\odot$  and  $r$  from  $7 \cdot 10^7$  cm to  $5 \cdot 10^{11}$  cm and obtained the turning points  $\Sigma^+$  and  $\Sigma^-$ ,  $T_{\text{eff}}^+$  and  $T_{\text{eff}}^-$ ,  $\dot{M}^+$  and  $\dot{M}^-$ , denoted below as ‘TP’, which define the upper and lower stable branches. The chemical composition is assumed to be solar, and convective energy transport is taken into account. We fit the resulting TPs as:

$$f(M, \alpha, r) = A \left( \frac{M}{M_\odot} \right)^\beta \alpha^\gamma \left( \frac{r}{10^{10} \text{ cm}} \right)^\delta, \quad (45)$$

where the parameters  $A, \beta, \gamma, \delta$  and average relative uncertainty of TPs can be found in Table 1. The average relative uncertainty  $\Delta$  is defined as

$$\Delta = \left\langle \frac{|f(M, \alpha, r) - \text{TP}|}{\text{TP}} \right\rangle_{M, \alpha, r}. \quad (46)$$

We find that these approximations of S-curves are close to the previous ones (see e. g., [Hameury et al. 1998](#); [Lasota et al. 2008](#); [Hameury 2020](#)). Comparing with results of [Lasota et al. \(2008\)](#), the average relative difference is 8.3% for  $T_{\text{eff}}^+$  and 14.5% for  $T_{\text{eff}}^-$ . There is a larger average relative difference for the surface density  $\Sigma_0$ : 24.5% and 25.4% for  $\Sigma^+$  and  $\Sigma^-$ , respectively. Taking into account that [Liu & Meyer-Hofmeister \(1997\)](#) have shown that the improved tabular opacities do not affect much the S-curves, we tend to conclude that uncertainties in  $\Sigma_0$  are partly related to the slightly different boundary condition for pressure at the disc surface. [Lasota et al. \(2008\)](#) used the boundary condition (25), while we use (20) instead. Other possible source of uncertainty is the EoS tables. [Lasota et al. \(2008\)](#) used tables from ([Fontaine et al. 1977](#)), while we use OPAL EoS tables ([Rogers & Nayfonov 2002](#)).

### 5.1 Irradiation and S-curves

Figure 11 illustrates the influence of external irradiation on the disc stability. Considering the S-curves, calculated through scheme (i) for different irradiation temperatures  $T_{\text{irr}}$ , we infer that the unstable branch shrinks with the increase of  $T_{\text{irr}}$ . For  $T_{\text{irr}} \gtrsim 12000$  K the unstable branch disappears, so the strong irradiation stabilizes the disc. This result is an agreement with previous ones (e.g. [Tuchman et al. 1990](#); [Dubus et al. 1999](#)), but the critical  $T_{\text{irr}}$  value (12000 K) is larger (the critical  $T_{\text{irr}}$  in previous studies  $\sim 10000$  K).

The disc calculated with advanced irradiation scheme (ii) and self-consistent X-ray luminosity (magenta line) loses its stability, when  $T_{\text{irr}} = T_{\text{irr, crit}} \approx 7500$  K,  $T_{\text{eff}} \approx 6600$  K and  $\dot{M} \approx 0.06 \dot{M}_{\text{edd}}$ . This critical value  $T_{\text{irr, crit}}$  is lower than the one obtained in method (i) and by ([Tuchman et al. 1990](#); [Dubus et al. 1999](#)). Furthermore, it depends on disc parameters, as we show in section 6, see also Fig. 15.

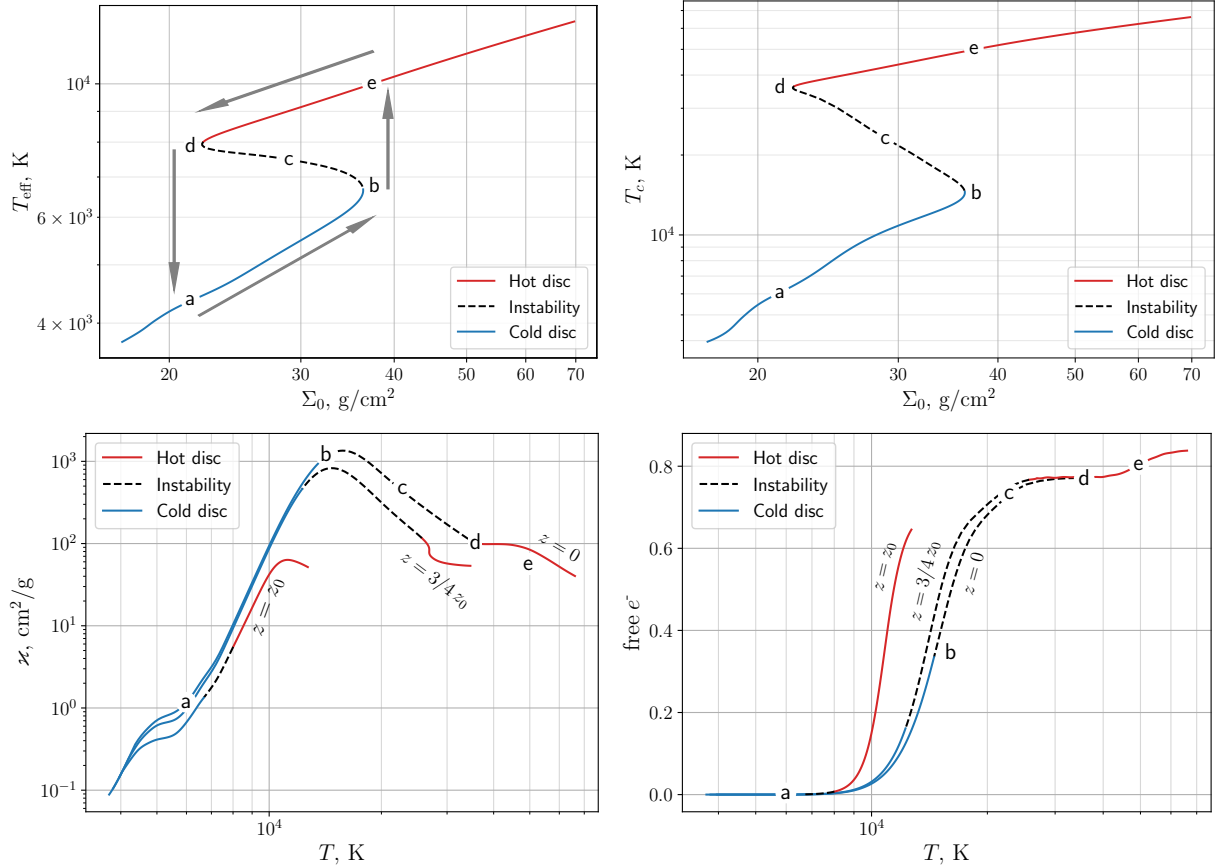


**Figure 10.** Top left: S-curve for  $M = 10 M_{\odot}$ ,  $\alpha = 0.1$ ,  $r = 10^{10}$  cm and tabular opacities with solar chemical composition. The limit cycle is schematically shown by arrows. Top right: the corresponding dependence of the symmetry plane temperature  $T_c$ . Bottom left: the opacity coefficient as a function of temperature at the symmetry plane of the disc ( $z = 0$ ), at the disc surface ( $z = z_0$ ) and in between ( $z = 3/4 z_0$ ). Bottom right: the corresponding dependence of the mean number of free electrons per nucleon (free  $e^- \equiv 1/\mu_e$ ) on temperature. The cold disc region, the region in which the instability takes place, and the region of the hot disc are marked with different style. In the unstable region, the free  $e^-$  at the centre changes from 0.4 to 0.77 (the full ionization in the hot disc corresponds to free  $e^- \sim 0.85$ ).

	$A$	$\beta$	$\gamma$	$\delta$	$\Delta$
$\Sigma^+$	$8.44 \pm 0.01 \text{ g cm}^{-2}$	$-0.3674 \pm 0.0006$	$-0.7821 \pm 0.0002$	$1.1105 \pm 0.0002$	3.3%
$\Sigma^-$	$11.87 \pm 0.03 \text{ g cm}^{-2}$	$-0.3723 \pm 0.0009$	$-0.8405 \pm 0.0003$	$1.1223 \pm 0.0003$	5.4%
$\dot{M}^+$	$(1.027 \pm 0.003) \cdot 10^{16} \text{ g s}^{-1}$	$-0.843 \pm 0.001$	$-0.0193 \pm 0.0004$	$2.6258 \pm 0.0003$	5.4%
$\dot{M}^-$	$(5.065 \pm 0.016) \cdot 10^{15} \text{ g s}^{-1}$	$-0.833 \pm 0.001$	$0.0066 \pm 0.0004$	$2.6038 \pm 0.0004$	6.5%
$T_{\text{eff}}^+$	$7341 \pm 2 \text{ K}$	$0.0290 \pm 0.0001$	$-0.00484 \pm 0.00004$	$-0.08426 \pm 0.00004$	0.7%
$T_{\text{eff}}^-$	$6152 \pm 4 \text{ K}$	$0.0315 \pm 0.0002$	$0.00165 \pm 0.00008$	$-0.08977 \pm 0.00007$	1.3%

**Table 1.** Values of the parameters (with standard deviations), which fit the S-curve turning points, where the ‘+’ and ‘-’ superscripts denote the upper and lower turning points, respectively. The right column contains the average relative uncertainty  $\Delta$  of the turning points.

## 5.2 Influence of chemical composition, $\alpha$ parameter and convection on the shape of S-curves in X-ray transients

Figures 12 and 13 show S-curves for different chemical composition and  $\alpha$  parameter. Curves with and without convection are also shown. The dots mark the regions where convection in the disc dominates (i.e. the condition for the existence of convection  $\nabla_{\text{rad}} > \nabla_{\text{ad}}$  is fulfilled in more than 50% over  $z$ ). It is seen that the disc is convective in the unstable region.

According to Faulkner et al. (1983), convection does not affect the very existence of instability. Indeed, we also obtain that, when the

convection is ignored in the calculation, there is one unstable branch, regardless of the chemical composition or  $\alpha$ .

When convection is taken into account, the instability starts at higher accretion rates. For large  $\alpha$ , regions with convection are ‘‘pulled’’ towards large  $\Sigma$ , and an almost vertical interval at lower unstable branch is formed. For small  $\alpha$ , the convective branch splits into two unstable branches. In this case, the upper unstable branch is due to a peak in opacity related to the partial ionization of hydrogen. The lower branch is associated with convection (Cannizzo 1992) and with the formation of molecular hydrogen (Smak 1982b), see small peak in opacity (Fig. 1) at  $T \approx 4000 - 5000$  K. This ‘wiggle’ is not

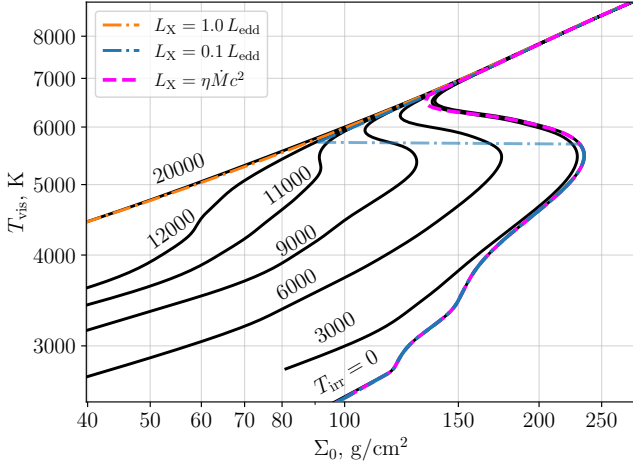


**Figure 11.** S-curves for irradiated discs. Black curves are calculated through scheme (i) with different irradiation temperatures  $T_{\text{irr}}$ . Coloured lines are the curves with irradiation, calculated with advanced scheme (ii). The magenta line corresponds to self-consistent luminosity of irradiation source  $L_X = \eta \dot{M} c^2$ , while the blue and orange lines corresponds to luminosities  $L_X = 0.1, 1.0 L_{\text{edd}}$ . Note that in case with  $L_X = 0.1 L_{\text{edd}}$  the negative slope branch is numerically unstable and cannot be calculated reliably, which leads to S-curve discontinuity. All curves are calculated for  $M = 1.4 M_{\odot}$ ,  $r = 3 \cdot 10^{10}$  cm,  $\alpha = 0.1$  and solar chemical composition.

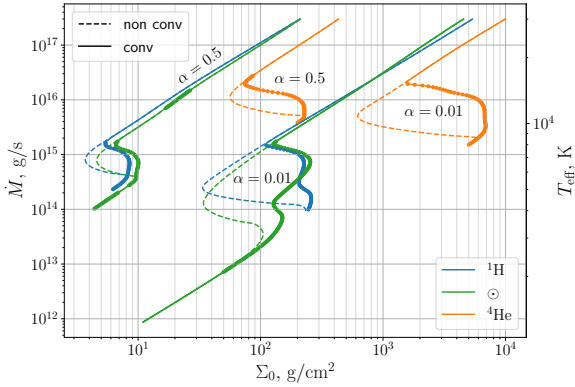


**Figure 12.** S-curves for different chemical composition,  $\alpha$ , with and without convection. All curves are calculated for  $M = 10 M_{\odot}$  and  $r = 10^{10}$  cm. Bold point regions are the zones where the disc is convective (i.e. the condition for the existence of convection  $\nabla_{\text{rad}} > \nabla_{\text{ad}}$  is fulfilled over an  $z$ -range of more than 50%). Note that only the optically thick branches of the curves are shown. For this reason, the curves for the helium and hydrogen disc do not show the area corresponding to the cold disc, since it is optically thin.

usually associated with the outburst mechanism since the  $\alpha$ -value is thought to change only when the ionization degree is changing. At large  $\alpha$ , the lower unstable branch does not appear, since the temperature does not reach such low values, at which the formation of molecules begins.

On the S-curve for helium disc, the instability is related with partial ionization of helium, so the corresponding temperatures are larger than for solar and hydrogen disc. At both large and small  $\alpha$ , the second unstable branch does not appear, only the main unstable branch is deformed.

These results for solar discs are consistent with the results in Cannizzo et al. (1982), where S-curves were investigated taking into

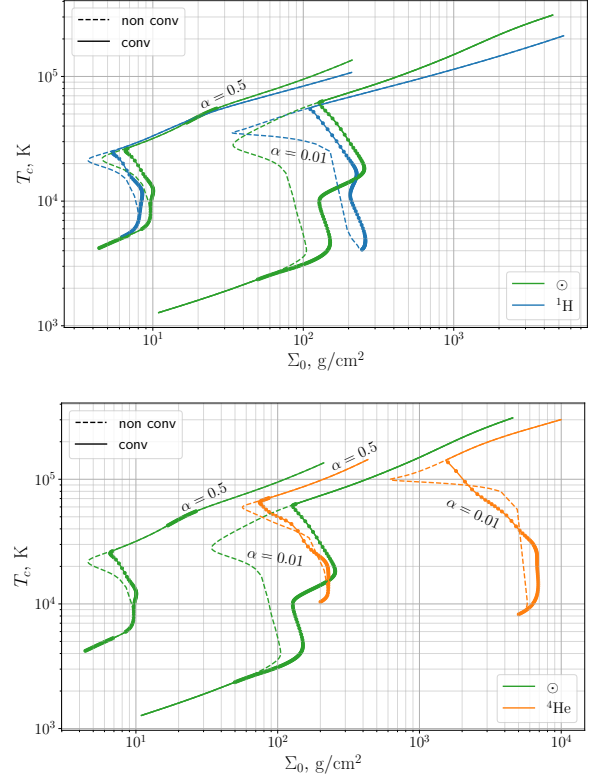


**Figure 13.**  $T_c - \Sigma_0$  dependencies for different chemical composition,  $\alpha$ , with and without convection. System parameters and notations are the same as in Fig. 12.

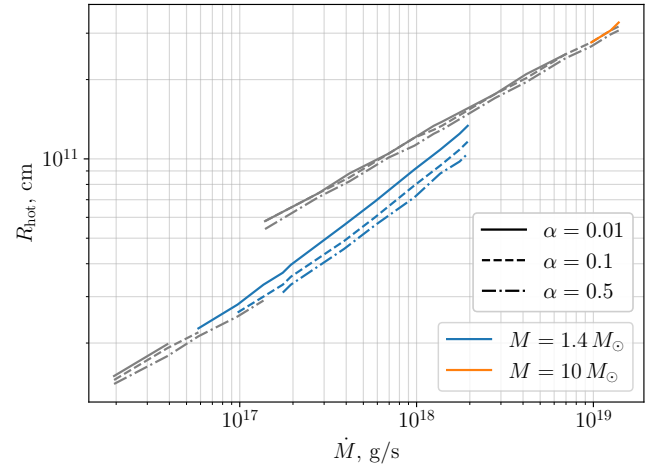


**Figure 14.** Outer radius of the hot disc  $R_{\text{hot}}$  as function of accretion rate  $\dot{M}$  for two central masses (different colors) and three  $\alpha$ -parameters (different styles). Cases, when external irradiation does not affect the disc stability and therefore does not affect the  $R_{\text{hot}}$ , are shown in grey.

account convection, which led to the appearance of additional kinks on the curve.

## 6 DISCUSSION

Predictions on the size of the hot stable part of an accretion disc are important in the context of understanding transient or persistent nature of X-ray sources, if one confronts the DIM model with observations. Such comparison relies on an unknown value of irradiation parameter, which, consequently, can be estimated as a result. For example, assuming the DIM model, [Coriat et al. \(2012\)](#) have analysed transient and persistent X-ray sources with neutron stars and black holes and concluded that irradiation parameter lies in the interval  $10^{-3} - 10^{-2}$ . This is an order of magnitude higher than the values obtained by us, see Fig. 9, and indicates that additional means of X-rays interception exist above the disc photosphere, for example, due to additional scattering of X-rays ([Suleimanov et al. 2007](#); [Mescheryakov et al. 2011](#)). For supersoft X-ray sources, [Suleimanov et al. \(2003\)](#) suggest that relatively dense blobs immersed in a corona enable multiple X-ray or far-UV scattering which leads to observed large optical and UV fluxes. The same mechanism might increase the irradiation parameter  $C_{\text{irr}}$ .

Having a robust lower limit on  $C_{\text{irr}}$  (Fig. 9), one can deduce a universal lower limit on the hot disc size in the framework of an irradiation-controlled disc model, see Fig. 14, where the minimum radius of the hot disc is shown versus the central accretion rate and  $L_x = \eta \dot{M} c^2$ . Two sets of curves are shown, for a neutron star, and a black hole of  $10 M_{\odot}$ . Grey parts of the curves denote the regime when irradiation with  $C_{\text{irr}}$  from Fig. 9 does not control the hot disc radius: the stability of the disc is ensured by internal viscous heat. Smaller hot discs are not possible.

The size of the hot disc is also important for an outburst dynamics, since it affects directly the characteristic time of an outburst. The decay time of an outburst, known from observations, corresponds to the viscous time-scale which grows with size of a disc and decreases with increasing  $\alpha$ -parameter (it also depends on the accretor’s mass). Thus, a lower-bound estimate on  $\alpha$ -parameter follows from the theoretical minimum of the hot disc radius. If a burst decay is fast, a large  $\alpha$ -value could result, which may indicate other mechanisms of disc evolution at work, for example, winds from discs ([Tetarenko et al. 2018](#); [Avakyan et al. 2022](#), in press).

It was shown before that there is a minimum irradiation temperature that ensures the disc stability ([Tuchman et al. 1990](#); [Dubus et al. 1999](#)), estimated as  $(9 - 10) \times 10^3$  K. While, as mentioned above, the actual  $C_{\text{irr}}$  can be higher comparing to the values we find, the critical disc irradiation temperature, which switches on/off ionization instability, can be reliably obtained, since it depends not on  $C_{\text{irr}}$  but on how much the irradiation flux exceeds the internal viscous one.

In Fig. 15 we show dependence of the critical irradiation temperature on the ratio of the irradiation to viscous heat. For this we have calculated numerous models of irradiated disc with scheme (ii), with arbitrary values of the central flux (to cover the scenarios of enhanced values of  $C_{\text{irr}}$ ).

For strongly illuminated discs, when  $Q_{\text{irr}} > Q_{\text{vis}}$ , irradiation controls the disc size, and thus, its evolution (e.g. [King & Ritter 1998](#)). This occurs for big discs and sufficiently high  $C_{\text{irr}}$ , suitably illustrated by a formula from [Suleimanov et al. \(2007\)](#):

$$\frac{Q_{\text{irr}}}{Q_{\text{vis}}} = \frac{4}{3} \eta C_{\text{irr}} \frac{r}{r_g}. \quad (47)$$

Thus, at radii  $r > 3/4 r_g / (\eta C_{\text{irr}})$  the stability condition is  $T_{\text{irr}} > T_{\text{irr,crit}}$ , see Fig. 15.

In the opposite case, if  $Q_{\text{irr}} < Q_{\text{vis}}$ , irradiation does not affect the disc structure and the disc stability: unstable state is triggered at the radius where the effective temperature lowers to  $T_{\text{eff}}^+$ . Grey intervals

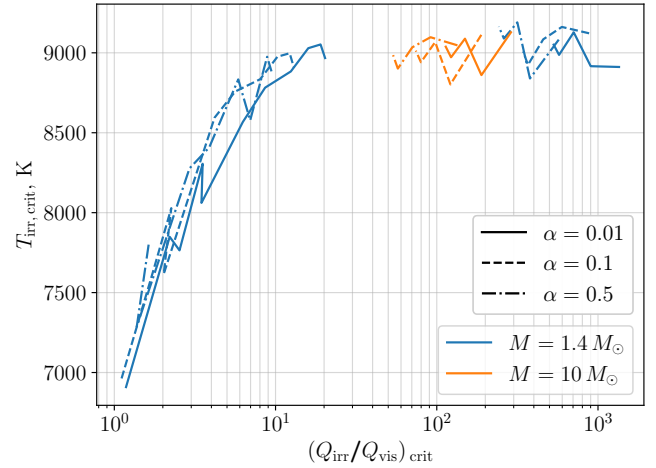


**Figure 15.** Critical value of irradiation temperature  $T_{\text{irr,crit}}$ , above which the disc is stable, as function of the ratio between irradiation and viscous heat  $Q_{\text{irr}}/Q_{\text{vis}}$  for two central source masses (different colors) and three  $\alpha$ -parameters (different styles). Irradiation is taken into account by method (ii). Note that weak irradiation does not affect the disc around  $10 M_{\odot}$ , so there is no  $T_{\text{irr,crit}}$  in this case.

in Fig. 14 show the hot disc size just for this case. This can happen in the case of relatively small discs or small  $C_{\text{irr}}$ .

## 7 SUMMARY

Calculation of the vertical structure of accretion discs is necessary to understand stability properties of accretion discs and to reconstruct the light curves of X-ray transients. Large range of physical conditions over a disc or various chemical composition in different objects require a numerical approach of calculating disc parameters, which is fast and flexible at the same time. Our first open numerical code for the model of the vertical structure with different types of equation of state and opacity laws, including tabular values, takes into account both radiative and convective energy transport and external X-ray irradiation. It is now possible to investigate the behavior of the ionization degree in the disc, in the zones of thermal instability, in particular

Using the results of numerical models, we obtain analytical formulas for radial dependencies of disc parameters applicable for the OPAL power-law approximation of opacity coefficient. They can be applied in the outermost parts of an ionized hot accretion disc around a stellar-mass compact object. At the same time, we suggest to calculate numerically the radial disc structure, since there is no simple criteria for the ‘OPAL’ zone.

A classical division of the disc into zones A, B and C is examined using results of the code. While analytic estimates of the boundaries between the zones A, B and C agree reasonably well with our results, the estimates for zone B\* is of less accuracy.

We analyse stability criteria for our disc model. For this, analytical approximations for the S-curve turning points are obtained. Comparing to previous results, variations in  $\Sigma_0$  turning points are explained by slightly different boundary condition for pressure at the disc surface and different EoS tables.

For a case with external X-ray irradiation, stabilization of the disc’s vertical structure at  $T_{\text{irr}} > 10^4$  K, previously found by [Tuchman et al. \(1990\)](#); [Dubus et al. \(1999\)](#), occurs in our models as well.

Using the advanced scheme of calculation of irradiation disc vertical structure, we refine the critical value of  $T_{\text{irr}}$  and find that it changes in range 6900 – 9000 K. We propose its unique dependence on the ratio between irradiation and viscous heat (Fig.15). In addition, we calculate values of self-irradiation parameter  $C_{\text{irr}}$  in our model. They represent lower estimates of the actual  $C_{\text{irr}}$  in X-ray transients, since additional heating and/or scattering from the hot layers above the disc photosphere should enhance the heating effect.

## ACKNOWLEDGEMENTS

The work was supported by the RSF grant 21-12-00141. The authors thank Valery Suleimanov for the comments.

## DATA AVAILABILITY

The pre-calculated S-curve turning points ( $\Sigma^+$  and  $\Sigma^-$ ,  $T_{\text{eff}}^+$  and  $T_{\text{eff}}^-$ ,  $\dot{M}^+$  and  $\dot{M}^-$ ) are available <sup>4</sup> for 20 linearly scaled values of  $M$  from  $1 M_{\odot}$  to  $20 M_{\odot}$ , 20 logarithmically scaled values of  $\alpha$  from  $3 \cdot 10^{-4}$  to 0.7, 20 logarithmically scaled values of  $r$  from  $7 \cdot 10^7$  cm to  $5 \cdot 10^{11}$  cm.

## REFERENCES

- Alexander D. R., 1975, *ApJS*, **29**, 363  
 Astropy Collaboration et al., 2013, *A&A*, **558**, A33  
 Astropy Collaboration et al., 2018, *AJ*, **156**, 123  
 Avakyan A. L., Lipunova G. V., Malanchev K. L., 2022, in press  
 Badnell N. R., Bautista M. A., Butler K., Delahaye F., Mendoza C., Palmeri P., Zeppen C. J., Seaton M. J., 2005, *MNRAS*, **360**, 458  
 Bagińska P., Różańska A., Czerny B., Janiuk A., 2021, *ApJ*, **912**, 110  
 Bell K. R., Lin D. N. C., 1994, *ApJ*, **427**, 987  
 Burderi L., King A. R., Szuszkiewicz E., 1998, *ApJ*, **509**, 85  
 Cannizzo J. K., 1992, *ApJ*, **385**, 94  
 Cannizzo J. K., Ghosh P., Wheeler J. C., 1982, *ApJ*, **260**, L83  
 Coriat M., Fender R. P., Dubus G., 2012, *MNRAS*, **424**, 1991  
 Cox A. N., Stewart J. N., 1969, *Nauchnye Informatsii*, **15**, 1  
 Cox A. N., Tabor J. E., 1976, *ApJS*, **31**, 271  
 Done C., Gierliński M., Kubota A., 2007, *A&ARv*, **15**, 1  
 Dubus G., Lasota J.-P., Hameury J.-M., Charles P., 1999, *MNRAS*, **303**, 139  
 Dubus G., Hameury J. M., Lasota J. P., 2001, *A&A*, **373**, 251  
 Esin A. A., Kuulkers E., McClintock J. E., Narayan R., 2000, *ApJ*, **532**, 1069  
 Faulkner J., Lin D. N. C., Papaloizou J., 1983, *MNRAS*, **205**, 359  
 Ferguson J. W., Alexander D. R., Allard F., et al., 2005, *ApJ*, **623**, 585  
 Fontaine G., Graboske H. C. J., van Horn H. M., 1977, *ApJS*, **35**, 293  
 Frank J., King A., Raine D. J., 2002, *Accretion Power in Astrophysics: Third Edition*  
 Hameury J. M., 2020, *Advances in Space Research*, **66**, 1004  
 Hameury J.-M., Menou K., Dubus G., et al., 1998, *MNRAS*, **298**, 1048  
 Hameury J. M., Viallet M., Lasota J. P., 2009, *A&A*, **496**, 413  
 Hōshi R., 1979, *Progress of Theoretical Physics*, **61**, 1307  
 Hunter J. D., 2007, *Computing in Science & Engineering*, **9**, 90  
 Iglesias C. A., Rogers F. J., 1993, *ApJ*, **412**, 752  
 Iglesias C. A., Rogers F. J., 1996, *ApJ*, **464**, 943  
 Jones E., Oliphant T., Peterson P., et al., 2001–2019, SciPy: Open source scientific tools for Python, <http://www.scipy.org/>  
 Kato S., Fukue J., Mineshige S., 2008, *Black-Hole Accretion Disks — Towards a New Paradigm —*  
 Ketsaris N. A., Shakura N. I., 1998, *Astronomical and Astrophysical Transactions*, **15**, 193

<sup>4</sup> <https://doi.org/10.5281/zenodo.7361425>

- King A. R., Ritter H., 1998, *MNRAS*, **293**, L42  
 Kippenhahn R., Weigert A., Weiss A., 2012, *Stellar Structure and Evolution*, [doi:10.1007/978-3-642-30304-3](https://doi.org/10.1007/978-3-642-30304-3).  
 Lasota J.-P., 2001, *New Astron. Rev.*, **45**, 449  
 Lasota J. P., Dubus G., Kruk K., 2008, *A&A*, **486**, 523  
 Lightman A. P., Eardley D. M., 1974, *ApJ*, **187**, L1  
 Lipunova G. V., Malanchev K. L., 2017, *MNRAS*, **468**, 4735  
 Lipunova G., Malanchev K., Tsygankov S., Shakura N., Tavleev A., Kolesnikov D., 2022, *MNRAS*, **510**, 1837  
 Liu B. F., Meyer-Hofmeister E., 1997, *A&A*, **328**, 243  
 Lyutyi V. M., Sunyaev R. A., 1976, *Soviet Ast.*, **20**, 290  
 Malanchev K. L., Shakura N. I., 2015, *Astronomy Letters*, **41**, 797  
 Malanchev K. L., Postnov K. A., Shakura N. I., 2017, *MNRAS*, **464**, 410  
 Meshcheryakov A. V., Shakura N. I., Suleimanov V. F., 2011, *Astronomy Letters*, **37**, 311  
 Meyer F., Meyer-Hofmeister E., 1981, *A&A*, **104**, L10  
 Meyer F., Meyer-Hofmeister E., 1982, *A&A*, **106**, 34  
 Morrison R., McCammon D., 1983, *ApJ*, **270**, 119  
 Paczyński B., 1969, *Acta Astron.*, **19**, 1  
 Papaloizou J., Faulkner J., Lin D. N. C., 1983, *MNRAS*, **205**, 487  
 Paxton B., Bildsten L., Dotter A., et al., 2011, *ApJS*, **192**, 3  
 Rogers F. J., Nayfonov A., 2002, *ApJ*, **576**, 1064  
 Schwarzschild M., 1958, *Structure and evolution of the stars*.  
 Shakura N. I., 1972, *Azh*, **49**, 921  
 Shakura N. I., Sunyaev R. A., 1973, *A&A*, **500**, 33  
 Shakura N. I., Sunyaev R. A., 1976, *MNRAS*, **175**, 613  
 Shakura N. I., Lipunova G. V., Malanchev K. L., et al., 2018, *Accretion flows in astrophysics*. New York, New York, [doi:10.1007/978-3-319-93009-1](https://doi.org/10.1007/978-3-319-93009-1)  
 Smak J., 1982a, *Acta Astron.*, **32**, 199  
 Smak J., 1982b, *Communications of the Konkoly Observatory Hungary*, **83**, 195  
 Smak J., 1984, *Acta Astron.*, **34**, 161  
 Suleimanov V., Meyer F., Meyer-Hofmeister E., 1999, *A&A*, **350**, 63  
 Suleimanov V., Meyer F., Meyer-Hofmeister E., 2003, *A&A*, **401**, 1009  
 Suleimanov V. F., Lipunova G. V., Shakura N. I., 2007, *Astronomy Reports*, **51**, 549  
 Suleimanov V. F., Lipunova G. V., Shakura N. I., 2008, *A&A*, **491**, 267  
 Tavleev A., Malanchev K., Lipunova G., 2019, in *The Multi-Messenger Astronomy: Gamma-Ray Bursts, Search for Electromagnetic Counterparts to Neutrino Events and Gravitational Waves*. pp 229–233, [doi:10.26119/SAO.2019.1.35553](https://doi.org/10.26119/SAO.2019.1.35553)  
 Tavleev A. S., Lipunova G. V., Malanchev K. L., 2022, in *Astronomy at the Epoch of Multimessenger Studies*. pp 302–303, [doi:10.51194/VAK2021.2022.1.1.116](https://doi.org/10.51194/VAK2021.2022.1.1.116)  
 Tetarenko B. E., Lasota J. P., Heinke C. O., Dubus G., Sivakoff G. R., 2018, *Nature*, **554**, 69  
 Tuchman Y., Mineshige S., Wheeler J. C., 1990, *ApJ*, **359**, 164  
 Walt S. v. d., Colbert S. C., Varoquaux G., 2011, *Computing in Science & Engineering*, **13**, 22  
 de Jong J. A., van Paradijs J., Augusteijn T., 1996, *A&A*, **314**, 484

## APPENDIX A: CONVECTION

If convection is present, we use mixing-length theory to obtain the temperature gradient  $\nabla_{\text{conv}}$  (see Paczyński 1969; Kippenhahn et al. 2012). It is assumed that convective elements travel characteristic path length called ‘mixing length’, after which they dissolve.

According to this theory the convective gradient  $\nabla_{\text{conv}}$ :

$$\nabla_{\text{conv}} = \nabla_{\text{ad}} + (\nabla_{\text{rad}} - \nabla_{\text{ad}})Y(Y + V), \quad (\text{A1})$$

where  $Y$  is the solution of cubic equation

$$\frac{9}{4} \frac{\tau_{\text{ml}}^2}{3 + \tau_{\text{ml}}^2} Y^3 + VY^2 + V^2Y - V = 0. \quad (\text{A2})$$

Here  $\tau_{\text{ml}} = \kappa_{\text{R}} \rho H_{\text{ml}}$  is the optical depth of convective vortex,

$H_{\text{ml}} = \alpha_{\text{ml}} H_P$  is the mixing length,  $H_P = P/(\rho\omega_K^2 z + \omega_K \sqrt{P\rho})$  is the pressure scale height, coefficient  $\alpha_{\text{ml}}$  is a free parameter, which usually lies in the interval [1, 2] for the solar chemical abundance. We use  $\alpha_{\text{ml}} = 1.5$ , following [Hameury et al. \(1998\)](#). Coefficient  $V$  is defined as

$$V^{-2} \equiv - \left( \frac{3 + \tau_{\text{ml}}^2}{3\tau_{\text{ml}}} \right)^2 \frac{C_P^2 H_{\text{ml}}^2 \rho^2 \omega_K^2 z}{512 \sigma_{\text{SB}}^2 T^6 H_P} (\nabla_{\text{rad}} - \nabla_{\text{ad}}) \left( \frac{\partial \ln \rho}{\partial \ln T} \right)_P, \quad (\text{A3})$$

where  $C_P$  is the specific heat at constant pressure.

Values of  $\nabla_{\text{ad}}$ ,  $C_P$ ,  $\left( \frac{\partial \ln \rho}{\partial \ln T} \right)_P$  are obtained from the eos module of the MESA code ([Paxton et al. 2011](#)). Notice that in presence of convection  $\nabla_{\text{rad}} > \nabla_{\text{conv}} > \nabla_{\text{ad}}$ .

## APPENDIX B: IRRADIATION FORMULAS

In this section we write the formulas that describe the irradiation terms in the advanced irradiation scheme (ii). Derivation of these formulas can be found in [Mescheryakov et al. \(2011\)](#).

Assume that the disc is irradiated by external X-rays with spectral flux  $F_X^{\nu}(\nu)$ . The angle between the direction of incidence of the X-ray photons and the inward normal to the disc layer surface is  $\theta_0$ , while the cosine of this angle we denote as  $\zeta_0 = \cos \theta_0$ .

The X-ray photons are scattered, absorbed and thermalized in the disc and can serve as additional heating source. The scattering in the medium is assumed to be coherent (Thomson scattering,  $\sigma = \sigma_{\text{T}}$ ), and the opacity coefficient  $\kappa^{\nu}$  for X-rays is determined by photoabsorption for a cold gas ([Morrison & McCammon 1983](#)).

The mean intensity  $J_{\text{tot}}^{\nu}$  and flux  $H_{\text{tot}}^{\nu}$  of both primary and scattered X-ray photons in the disc at some depth with corresponding  $\tau_{\nu}$  at frequency  $\nu$  can be found by solving the transfer equation in plane-parallel approximation:

$$J_{\text{tot}}^{\nu}(\tau^{\nu}, \nu) = \frac{F_X^{\nu}}{4\pi} \left\{ C^{\nu} \left[ e^{-k\tau^{\nu}} + e^{-k(\tau_0^{\nu} - \tau^{\nu})} \right] + (1 - D^{\nu}) \left[ e^{-\tau^{\nu}/\zeta_0} + e^{-(\tau_0^{\nu} - \tau^{\nu})/\zeta_0} \right] \right\}, \quad (\text{B1})$$

$$H_{\text{tot}}^{\nu}(\tau^{\nu}, \nu) = F_X^{\nu} \left\{ \frac{k C^{\nu}}{3} \left[ e^{-k\tau^{\nu}} - e^{-k(\tau_0^{\nu} - \tau^{\nu})} \right] + \left( \zeta_0 - \frac{D^{\nu}}{3\zeta_0} \right) \left[ e^{-\tau^{\nu}/\zeta_0} - e^{-(\tau_0^{\nu} - \tau^{\nu})/\zeta_0} \right] \right\}, \quad (\text{B2})$$

where  $\tau_0^{\nu}$  is the total optical depth of the disc in the vertical direction for X-ray radiation at frequency  $\nu$ ,  $\tau^{\nu} = \Sigma(\sigma + \kappa^{\nu})/2$ ,  $\kappa^{\nu}$  is the absorption coefficient for X-ray photons,  $\sigma$  is the scattering coefficient,  $k = \sqrt{3(1 - \lambda)}$  and  $\lambda = \sigma/(\sigma + \kappa^{\nu})$  is the single-scattering albedo. Formulas for  $C^{\nu}$  and  $D^{\nu}$  can be found in [Mescheryakov et al. \(2011\)](#).

The additional heating of the disc by X-ray photons of a given frequency  $\varepsilon^{\nu}$  is proportional to their mean intensity:

$$\varepsilon^{\nu} = 4\pi\rho\kappa^{\nu} J_{\text{tot}}^{\nu}. \quad (\text{B3})$$

The local energy release in the disc through its irradiation by X-ray photons is

$$\varepsilon = \int_0^{\infty} \varepsilon^{\nu} d\nu = 4\pi\rho \int_0^{\infty} \kappa^{\nu} J_{\text{tot}}^{\nu} d\nu. \quad (\text{B4})$$

The flux  $H_{\text{tot}}^{\nu}$  is calculated for all solid angles and it takes into account photons coming into the disc from outside minus those escaping the disc without absorption. Thus, the total heating of the disc

from the disc surface to the central plane through its irradiation is

$$Q_{\text{irr}}(z_0) = \int_0^{\infty} H_{\text{tot}}^{\nu}(\tau_{\text{ph}}^{\nu}, \nu) d\nu, \quad (\text{B5})$$

where  $\tau_{\text{ph}}^{\nu} = (\sigma + \kappa^{\nu})\Sigma_{\text{ph}}$  is the optical depth of the photosphere layers above the disc surface,  $\Sigma_{\text{ph}}$  is the corresponding column density. To find it we can write (cf. (18-19))

$$d\Sigma_{\text{ph}} = -\rho dz = \frac{d\tau}{\kappa_{\text{R}}} \quad (\text{B6})$$

and take the value, evaluated at  $z_0$ , which corresponds to  $\tau = 2/3$ :

$$\Sigma_{\text{ph}} = \frac{2}{3} \frac{1}{\kappa_{\text{R}}(P(z_0), T(z_0))} = \frac{P'}{\omega_K^2 z_0}. \quad (\text{B7})$$

It should be noted that photospheric column density  $\Sigma_{\text{ph}}$  is not included into the surface density  $\Sigma_0$  of the disc when we calculate S-curves.

The irradiation temperature and irradiation parameter can be found from the irradiation flux:

$$Q_{\text{irr}}(z_0) = \sigma_{\text{SB}} T_{\text{irr}}^4 = C_{\text{irr}} \frac{L_X}{4\pi r^2}, \quad (\text{B8})$$

where  $L_X$  is the X-ray luminosity of the central source.

Notice that  $\varepsilon$  is the function of  $\Sigma$ , that is, the function of the vertical coordinate  $z$ . The total X-ray optical depth is  $\tau_0^{\nu} = (\sigma + \kappa^{\nu})(\Sigma_0 + 2 \cdot \Sigma_{\text{ph}})$ . Therefore, irradiation terms  $\varepsilon$  and  $Q_{\text{irr}}$  (as well as  $T_{\text{irr}}$  and  $C_{\text{irr}}$ ) contain the surface density  $\Sigma_0$  as an additional free parameter, so the system of equations for the disc vertical structure in irradiation scheme (ii) have two free parameters:  $z_0$  and  $\Sigma_0$ .

Using (B2), (B5), (B8) and (31), we can obtain exact formula:

$$C_{\text{irr}} = \frac{\int_0^{\infty} F_X^{\nu} \{ \dots \} d\nu}{\int_0^{\infty} F_X^{\nu} d\nu} = \int_0^{\infty} S(\nu) \{ \dots \} d\nu, \quad (\text{B9})$$

where expression in  $\{ \dots \}$  is the one from the (B2). For a very optically thick disc with  $\tau_0^{\nu} \gg 1$ , exponential terms with  $\tau_0^{\nu}$  tend to zero, and it can be shown that  $C_{\text{irr}} \propto \zeta_0$ . If additionally we assume  $\Sigma_{\text{ph}} = 0$ , then  $\tau_{\text{ph}}^{\nu} = 0$ , and we obtain

$$C_{\text{irr}} = \left( 1 - \int_0^{\infty} S(\nu) \frac{3\lambda}{(1 + k\zeta_0)(3 + 2k)} d\nu \right) \zeta_0, \quad (\text{B10})$$

or, for single-frequency incoming X-ray photons,  $C_{\text{irr}} = (1 - A)\zeta_0$ , where the frequency-dependent albedo  $A$  is defined following [Mescheryakov et al. \(2011\)](#).

Moreover, one could introduce a notion of a spectrum-integrated albedo:

$$A^* = \int_0^{\infty} S(\nu) \frac{3\lambda}{(1 + k\zeta_0)(3 + 2k)} d\nu. \quad (\text{B11})$$

## APPENDIX C: VERTICAL STRUCTURE OF IRRADIATED DISCS

Figures C1 and C2 show examples of the vertical structure for irradiated disc together with un-irradiated case at two radii  $r = 2 \cdot 10^{10}$  and  $7 \cdot 10^{10}$  cm. Other system parameters are the same as in Fig. 6:  $M = 1.4 M_{\odot}$ ,  $\alpha = 0.1$ ,  $L_X = \eta \dot{M} c^2$ ,  $\eta = 0.1$ ,  $\dot{M} = 10^{18} \text{ g s}^{-1} \approx 0.5 \dot{M}_{\text{edd}}$ , the chemical composition is solar. Shown are distributions of mass coordinate  $\Sigma$ , temperature  $T$ , flux  $Q$ , temperature gradient  $\nabla$  and adiabatic temperature gradient  $\nabla_{\text{ad}}$ . Irradiation is taken into account through two methods (i) and (ii), see Sect. 2.4.

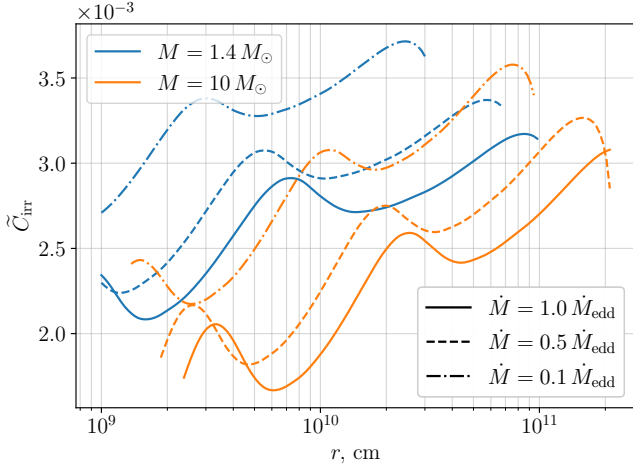


**Figure B1.** Radial profile of  $\tilde{C}_{\text{irr}}$ , system parameters and notations are the same as in Fig. 7. It is clearly seen, that this value almost does not change over radius (it changes by a factor of  $\sim 1.5$  by two orders of magnitude along the radius).

Irradiation temperature  $T_{\text{irr}}$  is obtained in advanced method (ii) and serves as input parameter in method (i).

It is clearly seen that at  $r = 2 \cdot 10^{10}$  cm the external irradiation almost does not affect the disc structure, although irradiation temperature  $T_{\text{irr}} = 17300$  K  $>$   $14840$  K  $= T_{\text{vis}}$ . This agrees with a requirement for the disc inner structure to be dominated by irradiation (Lyutiy & Sunyaev 1976; Dubus et al. 1999):

$$\frac{Q_{\text{irr}}}{Q_{\text{vis}}} = \frac{T_{\text{irr}}^4}{T_{\text{vis}}^4} > \tau_0. \quad (\text{C1})$$

For model in Fig. C1,  $Q_{\text{irr}}/Q_{\text{vis}} \approx 1.85$  and total optical depth  $\tau_0 \approx 4000$ , so at  $r = 2 \cdot 10^{10}$  cm the irradiation does not penetrate deep into the disc and heats only near-surface layers, which is seen on the flux dependency in Fig. C1. Energy in disc is transferred mostly by radiation (see the upper right panel).

On the contrary, at  $r = 7 \cdot 10^{10}$  cm un-irradiated disc is unstable and fully convective, but irradiation stabilizes the disc structure and makes the disc thicker. In this case  $T_{\text{irr}} = 9700$  K  $>$   $5800$  K  $= T_{\text{vis}}$ . The convection disappears in the irradiation-stabilized disc.

In that case the irradiation affects the whole disc in the vertical direction, which is clearly seen on the temperature dependency in Fig. C2. This is in disagreement with the criterion (C1), where  $\tau_0 > 10^3$ , and  $Q_{\text{irr}}/Q_{\text{vis}} \approx 8$  for disc region in Fig. C1. The reason is that relation (C1) is derived in the diffusion approximation of radiative transfer, which breaks in the presence of strong convective energy transport.

#### APPENDIX D: BRIEF CODE DESCRIPTION

Main input parameters of the Python 3 code, that solves equations of vertical structure, are: mass of central object  $M$ , radius  $r$ , the viscous torque  $F$ , type of opacity (Kramers, BellLin or MESA) and EoS (ideal gas with a given molecular weight  $\mu$  or MESA with user-defined chemical composition), turbulence parameter  $\alpha$ . Also code contains several functions, that calculate S-curves and radial profile of stationary disc.

If irradiation takes place, there are two cases:

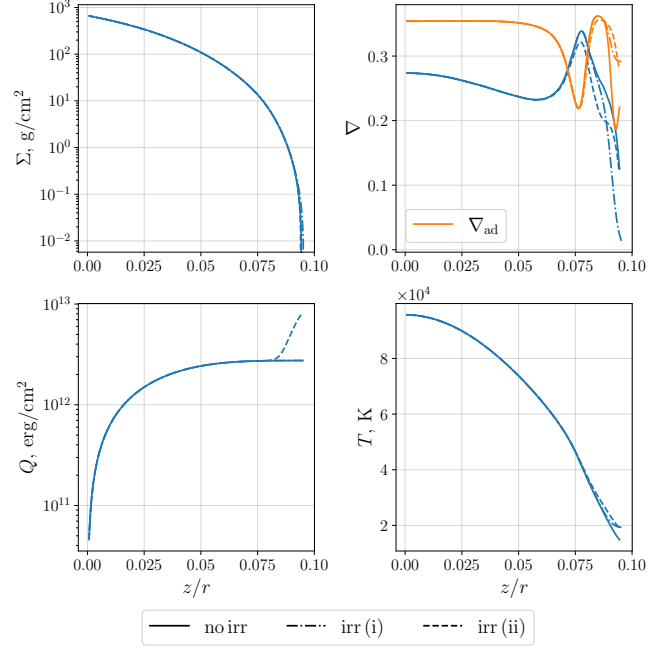


**Figure C1.** Vertical structure of irradiated disc together with un-irradiated case for  $M = 1.4 M_{\odot}$ ,  $\alpha = 0.1$ ,  $r = 2 \cdot 10^{10}$  cm and tabular opacity for accretion rates  $\dot{M} = 10^{18}$  g s $^{-1}$ . Shown are mass coordinate  $\Sigma$ , temperature  $T$ , temperature gradient  $\nabla$ , adiabatic gradient  $\nabla_{\text{ad}}$ , and energy flux  $Q$ . Irradiation is taken into account through two approaches (i) and (ii), where  $L_X = \eta \dot{M} c^2$ . Irradiation temperature  $T_{\text{irr}} = 17300$  K is obtained from calculations by method (ii) and serves as input parameter in method (i). The corresponding  $C_{\text{irr}} = 2.84 \cdot 10^{-4}$ .

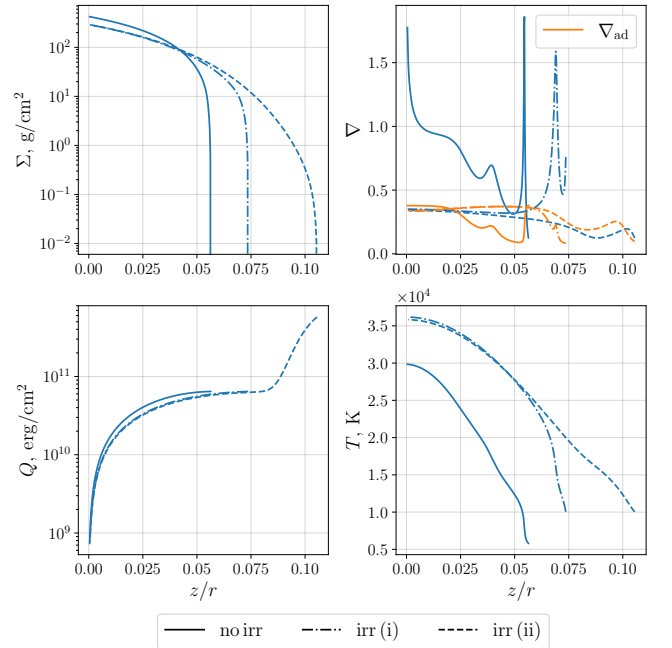


**Figure C2.** Vertical structure of irradiated disc together with un-irradiated case. System parameters and notations are the same as in Fig. C1, but the radius  $r = 7 \cdot 10^{10}$  cm. The obtained  $T_{\text{irr}} = 9700$  K, and corresponding  $C_{\text{irr}} = 3.49 \cdot 10^{-4}$ .

(i) If irradiation is described in terms of  $T_{\text{irr}}$  or  $C_{\text{irr}}$ , then the code has one additional input parameter – irradiation temperature  $T_{\text{irr}}$  or irradiation constant  $C_{\text{irr}}$ .

(ii) If irradiation is described through the advanced scheme, the external irradiation flux is given by Eq. (31), and the code has a few more input parameters: the X-ray luminosity of central source  $L_X$ ; the spectrum  $S(\nu)$  in form of table values (normalized over the entire frequency range to unity) or as a Python function; cosine of the incident angle  $\cos \theta_0$  as a fixed value or as a fixed value in the brackets in function (see also Eq. (42)):

$$\cos \theta_0 = \frac{z_0}{r} \left( \frac{d \ln z_0}{d \ln r} - 1 \right). \quad (\text{D1})$$

Note that the calculated vertical structure of a disc ring without irradiation differs to minor extent when we use alternative boundary conditions on pressure: (20) and (25). The first boundary condition is implemented as described in section 2.1. The second variant can be engaged in irradiated-disc scheme (ii) with  $C_{\text{irr}} = 0$  or  $T_{\text{irr}} = 0$ .

Code is open-source and available with detailed documentation on GitHub<sup>5</sup>. Scipy (Jones et al. 2019), Numpy (Walt et al. 2011), Matplotlib (Hunter 2007) and Astropy (Astropy Collaboration et al. 2013, 2018) packages are used in the code.

## APPENDIX E: CALCULATION DETAILS

Since the code integrates a system of differential equations, it is convenient to use dimensionless quantities by the order of unity. We achieve this by normalizing  $P, Q, T, \Sigma$  on their characteristic values  $P_0, Q_0, T_0, \Sigma_{00}$ , and replacing  $z$  on  $\hat{z} = 1 - z/z_0$ . The obtained dimensionless system is as follows:

$$\begin{aligned} \frac{d\hat{P}}{d\hat{z}} &= \frac{z_0^2}{P_0} \omega_K^2 \rho (1 - \hat{z}) & \hat{P}(0) &= P'/P_0, \\ \frac{d\hat{\Sigma}}{d\hat{z}} &= 2 \frac{z_0}{\Sigma_{00}} \rho, & \hat{\Sigma}(0) &= 0, \\ \frac{d\hat{T}}{d\hat{z}} &= \nabla \frac{\hat{T}}{\hat{P}} \frac{d\hat{P}}{d\hat{z}}, & \hat{T}(0) &= T_{\text{eff}}/T_0, \\ \frac{d\hat{Q}}{d\hat{z}} &= -\frac{3}{2} \frac{z_0 P_0}{Q_0} \omega_K \alpha \hat{P} & \hat{Q}(0) &= 1, \quad \hat{Q}(1) = 0, \end{aligned} \quad (\text{E1})$$

where  $\hat{P}, \hat{\Sigma}, \hat{T}, \hat{Q}$  are dimensionless functions of  $\hat{z}$ . Note that  $\nabla$  is the temperature gradient (5), and the surface density of disc  $\Sigma_0 = \hat{\Sigma}(1) \cdot \Sigma_{00}$ .

Characteristic values of pressure, temperature and mass coordinate are as follows:

$$T_0 = \frac{\mu}{\mathcal{R}} \omega_K^2 z_0^2, \quad P_0 = \frac{4}{3} \frac{Q_0}{\alpha z_0 \omega_K}, \quad \Sigma_{00} = \frac{28}{3} \frac{Q_0}{\alpha z_0^2 \omega_K^3}. \quad (\text{E2})$$

If external irradiation is present, the boundary condition for temperature  $\hat{T}$  changes:

$$\hat{T}(0) = \frac{1}{T_0} \left( T_{\text{vis}}^4 + T_{\text{irr}}^4 \right)^{1/4}. \quad (\text{E3})$$

If external irradiation is dealt with using the advanced scheme (ii), following equations and boundary conditions change their view:

$$\begin{aligned} \frac{d\hat{Q}}{d\hat{z}} &= -\frac{3}{2} \frac{z_0 P_0}{Q_0} \omega_K \alpha \hat{P} - \varepsilon \frac{z_0}{Q_0} & \hat{Q}(0) &= 1 + \frac{Q_{\text{irr}}}{Q_0}, \\ & & \hat{\Sigma}(1) &= \frac{\Sigma_0}{\Sigma_{00}}. \end{aligned} \quad (\text{E4})$$

Description of  $\varepsilon, Q_{\text{irr}}$  and  $T_{\text{irr}}$  terms in case of advanced irradiation scheme can be found in Appendix B.

The free parameter  $z_0$  is found using so-called shooting method. Code integrates system (E1) with initial approximation of free parameter  $z_0$ , then changes its value and integrates the system in order to fulfill the additional condition for flux  $\hat{Q}(1)$  at the symmetry plane of the disc. In the presence of external irradiation in scheme (i), the only change is the boundary condition for temperature (E3). If irradiation is calculated through the advanced scheme, code integrates system (E1) changed according to (E3) and (E4) and solve two-parameter ( $z_0, \Sigma_0$ ) optimization problem in order to fulfill both  $\hat{Q}(1)$  and  $\hat{\Sigma}(1)$  additional boundary conditions. Namely, code minimises function:

$$\begin{cases} f(z_0) = \hat{Q}(1) & \text{without irradiation;} \\ f(z_0, \Sigma_0) = \hat{Q}(1)^2 + \left( \frac{\hat{\Sigma}(1)\Sigma_{00}}{\Sigma_0} - 1 \right)^2 & \text{with irradiation.} \end{cases} \quad (\text{E5})$$

This paper has been typeset from a  $\text{\TeX}/\text{\LaTeX}$  file prepared by the author.

<sup>5</sup> <https://github.com/AndreyTavleev/DiscVerSt>